Advanced Steel Construction – Vol. 19 No. 3 (2023) 223–241
DOI:10.18057/IJASC.2023.19.3.4

A GENERALIZED METHOD FOR SHEAR CORRECTION FACTORS OF ARBITRARY THIN-WALLED SECTIONS

Yue-Yang Ding [1], Lun-Hua Bai [1, 2, *], Wen-Feng Chen [1], Yao-Peng Liu [1, 3] and Siu-Lai Chan [1]

[1] *Department of Civil and Environmental Engineering, The Hong Kong Polytechnic University, Hong Kong, China*
[2] *School of Transportation, Civil Engineering & Architecture, Foshan University, Foshan, China*
[3] *NIDA Technology Company Limited, Hong Kong Science Park, Shatin, N.T., Hong Kong, China*
** (Corresponding author: E-mail: bailunhua@163.com)*

ABSTRACT

Shear deformation may significantly affect the structural behaviours, especially for the structural members with small span-to-depth ratios. It is vital to consider the shear effects in the Direct Analysis Method (DAM) of thin-walled structures such that only the section capacity check is required in the evaluation of both member and system stability. However, there is lack of a general method to determine the shear correction factors of thin-walled cross-sections in various shapes and as a result DAM cannot be applied to the structures adopting these cross-sections. This paper proposes an innovative one-dimensional warping element model method to compute the shear correction factors of arbitrary thin-walled sections such as single open and closed sections, built-up sections, and large box sections with stiffeners. Also, the thin-walled cross-sections with non-uniform thickness can be considered by the proposed method. Several examples are investigated to validate the accuracy and efficiency of the proposed method against the analytical solution, conventional warping area element method and section analysis in ANSYS. Thus, this work provides a simple and practical method for direct analysis of thin-walled structures made of complex cross-sections with consideration of shear deformation.

ARTICLE HISTORY

Received: 2 February 2022
Revised: 13 September 2022
Accepted: 21 October 2022

KEYWORDS

Shear correction factor;
Thin-walled section;
Built-up section;
Taper plate;
One-dimensional warping element

1. Introduction

Thin-walled members are widely used in the construction of building and bridge structures owing to their advantages of light weight, material saving, excellent stiffness and high strength. When the thin-walled members with a relatively small span-to-depth ratio are adopted in the engineering structures such as box girder bridges and long-span spatial structures (Bai *et al.* 2021; Shen *et al*. 2019; Ljubinkovic *et al*. 2019; Liu *et al*. 2018), the influence of shear deformation increases and therefore the beam-column elements based on the Euler-Bernoulli theory cannot provide accurate prediction. To this point, the beam-column elements based on Timoshenko theory considering shear deformation attract considerable attention worldwide (Saritas *et al.* 2009; Dikaros *et al.* 2016; Ding *et al.* 2018; Franza *et al.* 2020; Wang *et al.* 2014; Tao *et al.* 2014; Zhuge *et al.* 2020; Bai *et al.* 2020; Du *et al*. 2019; Tang *et al*. 2022). It is vital to consider the shear effects in the Direct Analysis Method (DAM) of thin-walled structures for better prediction of structural behaviours such that only the section capacity check is required in the evaluation of both member and system stability (Du *et al*. 2019; Tang *et al*. 2022) without use of the conventional effective length method (ELM). The ELM is based on linear analysis with many limitations as discussed by Chan *et al.* (2005). However, there is lack of general method to determine the shear correction factors of thin-walled cross-sections in various shapes when using Timoshenko beam-column elements and as a result DAM cannot be applied to this kind of structures with the cross-sections in various shapes.

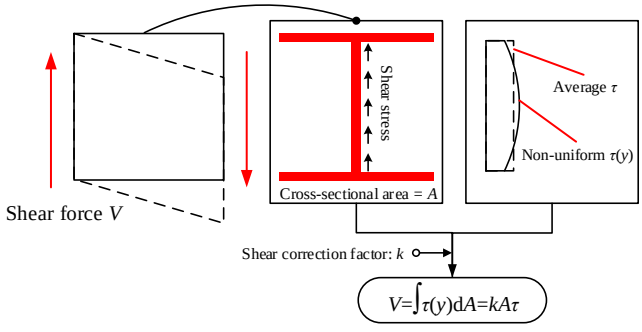

Fig. 1 Shear correction factor for non-uniformly distributed shear stress

The shear correction factor is widely used to represent the non-uniformly distributed shear stresses in a cross-section when using a beam-column model for global structural analysis. As illustrated in Fig. 1, the actual shear effect can be replaced by average shear stress multiplying by shear correction factor and the cross-sectional area.

For thin-walled members with a small span-to-depth ratio, the Timoshenko beam-column model allowing for shear deformations has been continuously improved, including the force-based and displacement-based elements. Du *et al.* (2019) proposed a novel flexibility-based beam-column element considering both shear deformation and member initial imperfection, as well as material nonlinearity by the fiber section method. Bai *et al.* (2020) presented a mixed beam-column element considering shear deformation for taper I-section member. Based on the point precise element (PEP) proposed by Chan *et al*. 1994, Tang *et al.* (2022) put forward an improved PEP element considering shear deformation and member initial imperfection. The mentioned new Timoshenko beam-column models provide excellent results. Paolo *et al.* (2018, 2021) proposed a mixed 3D beam element to consider shear deformation based on the warping displacement field of the cross sections. However, the traditional beam-column elements cannot account for both shear deformations and initial member imperfection, which are compulsively required in direct analysis.

Extensive works on Timoshenko beam-column models are also found in conventional nonlinear analysis focused on material nonlinearity. A fiber beam model considering slab spatial composite effect proposed by Tao *et al*. (2014) is based on the Timoshenko beam-column element in the commercial software Msc.Marc. Similarly, several fiber beam-column models are proposed by Ding *et al.* (2018) for reinforced concrete coupling beam and steel link beam with consideration of nonlinear shear behaviors in Msc.Marc. Wang *et al*. (2014) adopted the commercial software ABAQUS to implement a novel beam-column element for circular concrete filled steel tube considering torsional effect.

Note that the above works are mainly for the structural members using regular shape cross-sections, in which the shear correction factors for prediction of shear effect can be determined by analytical methods. Generally speaking, the previous research on Timoshenko beam-column models which use shear correction factors to include shear effects is limited to some typical shapes such as circular sections, rectangular sections, I-shape sections, box sections and Tee sections. There is an urgent need to develop a general method for determination of shear correction factors of thin-walled sections with various shapes, complicated box sections with extensive stiffeners, built-up sections, etc. Otherwise, the Timoshenko beam-column elements with excellent performance as reported in existing literature, such as Du *et al.* (2019) and Tang *et al.* (2022), cannot be used to predict the structural behaviors of the structures with unusual shape of cross-sections when the shear deformation becomes dominant.

Previous research on shear correction factors mainly focuses on the analytical solutions for simple shape sections (Timoshenko 1921, 1970; Love 1944; Herrmann 1965; Cowper 1966; Stephen 1980, 2001; Hutchinson 2001), numerical methods for more complicated sections (Krahula 1969; Karan 1979; Schramm *et al.* 1994; Friedman *et al.* 2000; Gruttman *et al.* 1999, 2001; Dong *et al*. 2010, 2013; Fialko *et al.* 2013), and experimental study for rectangular sections (Puchegger *et al.* 2003). Generally, the analytical methods and the experimental methods are limited to single regular sections. Also, the experimental method has both cost and time implication and therefore it is limited to research purpose. The numerical methods are mainly based on the fiber section approach, in which the section should be meshed into a number of triangular or quadrilateral shape fibers. This kind of methods requires reliable meshing algorithm. For thin-walled sections in irregular shape, extensive fibers may be induced and as a result the calculation process becomes time-consuming. Most importantly, the fiber-based method cannot be applied to the sections with several discontinuous areas like compound sections, which are widely used in steel structures.

In this paper, a generalized numerical method is proposed for determination of the shear correction factors of thin-walled sections in various shapes. Both the open and closed thin-walled sections using uniform or non-uniform thickness can be taken into account. This method is also applicable to complicated box sections with extensive stiffeners and built-up sections. Karan (1979) and Gruttman (1999, 2001) introduced a simple model, i.e., a cantilever beam subjected to free-end concentrated force, to study the shear deformation of structural members. Their method is essentially a fiber-based approach, in which the cross section is simulated by several plane warping area elements as indicated in Fig. 2(a). The drawbacks as discussed above such as time-consuming and continuous sectional areas only will limit the applications of this kind of methods in more complicated cases. Thus, a new one-dimensional element method allowing for warping effect is proposed here to calculate the shear correction factors of thin-wall sections in general cases, as shown in Fig. 2(b).

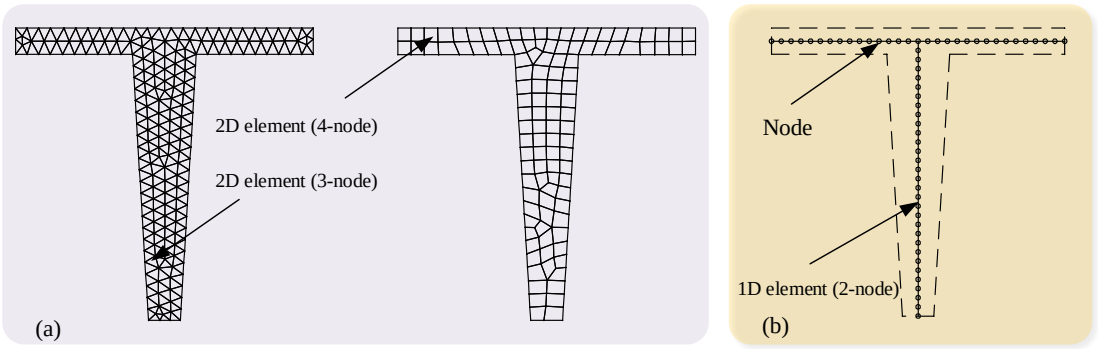

Fig. 2 Two numerical methods for shear correction factors: (a) Traditional 2D element model; (b) Proposed 1D element model

It is also found that few research is carried out on the determination of the shear correction factors of built-up sections composed of several single sections such as angles and channels connected with fasteners. An equivalent plate thickness method will be also developed to fill this gap.

In the proposed one-dimensional element model, the change of shear stress along the plate thickness is ignored as this kind of stress is not dominant in the thin-walled sections. The method is implemented in the program NIDA. Finally, several examples for the commonly used thin-walled sections are investigated for validation and demonstration.

2. One-dimensional warping element model method

The cantilever beam subjected to concentrated loads at the free end as shown in Fig. 3 is widely used to study the shear correction factors of cross sections. The force V_y is for the analysis of bending about x-axis to find shear center x_{sc} and shear correction factor k_{yy}. Similarly, the force V_x is for the analysis of the flexural behavior about y-axis to determine shear center y_{sc} and shear correction factor k_{xx}. Note that k_{xx} is along x-axis caused by V_x, while k_{yy} is along y-axis induced by V_y. The detailed derivation of proposed one-dimensional element for calculation of shear correction factors are presented as follows.

It should be noted that the cantilever beam model for derivation of shear center and shear correction factors is extensively adopted due to the shear forces along the length of the member being constant. By using this model, the displacement functions have simple forms for integral, leading to simpler element formulations than the simple beam and continuous beam models.

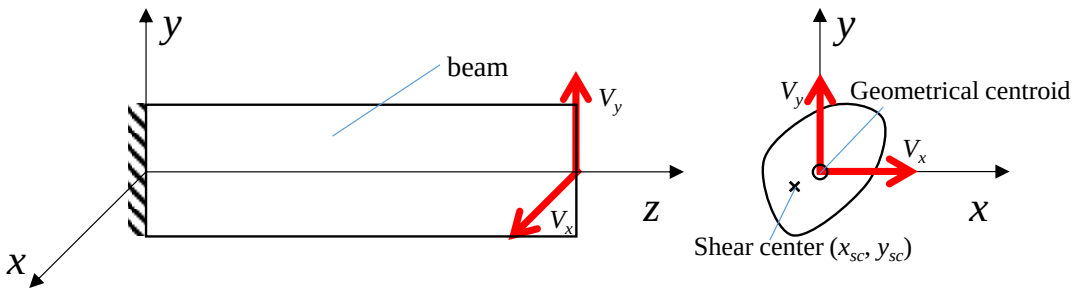

Fig. 3 Cantilever beam model for study of shear correction factors

2.1. Assumptions

The assumptions are used in this study: (1) the plane section is not required to remain plane with the consideration of the warping along the section; (2) the material is isotropic and linearly elastic; (3) the influence on the geometrical section properties due to section deformation is ignored; (4) the contribution of St. Venant torsional effect on lateral deflection is ignored; (5) the direct stress state is the same as the section subjected to pure bending moments; (6) the change of the shear stress along the plate thickness is ignored, which is acceptable for thin-walled sections; and (7) both the global and local buckling effects are ignored.

Note that, the first assumption illustrates that the cross section is not a rigid plane such that the non-uniform shear stress distribution along the cross section can be captured. The shear correction factors are widely used in conjunction with the Timoshenko beam-column elements so that the numerical efficiency of global structural analysis will be significantly enhanced. The complicated shear stress distribution has been simplified by using shear correction factors.

2.2. Shear correction factors

The displacement field of the cantilever beam as shown in Fig. 3 can be expressed as (Karan 1979):

$$u(x,y,z)=u_b+u_s$$
$$=\underbrace{\left(\frac{1}{2}Lz^2-\frac{1}{6}z^3\right)C_x}_{u_b}+\underbrace{\mu(L-z)\left[\frac{1}{2}C_x\left(x^2-y^2\right)+C_yxy\right]+a_2z+a_4}_{u_s} \tag{1}$$

$$v(x,y,z)=v_b+v_s$$
$$=\underbrace{\left(\frac{1}{2}Lz^2-\frac{1}{6}z^3\right)C_y}_{v_b}+\underbrace{\mu(L-z)\left[\frac{1}{2}C_y\left(y^2-x^2\right)+C_xxy\right]+a_1z+a_3}_{v_s} \tag{2}$$

$$w(x,y,z)=w_b+w_s$$
$$=\underbrace{-\left(Lz-\frac{1}{2}z^2\right)\left(C_xx+C_yy\right)}_{w_b}+\underbrace{\phi(x,y)-a_1y-a_2x}_{w_s} \tag{3}$$

where, u, v, and w represent the displacement along x-, y-, and z-axis, respectively; u_b, v_b, and w_b represent the displacement caused by the related bending moment; u_s, v_s, and w_s are the displacement caused by the related shear force; μ is Poisson's ratio; $\phi(x,y)$ is the warping function, and L is the length of the beam. C_x and C_y are the coefficients given by:

$$C_x=\frac{V_xI_{xx}-V_yI_{xy}}{E\left(I_{xx}I_{yy}-I_{xy}{}^2\right)} \tag{4}$$

$$C_y=\frac{V_yI_{yy}-V_xI_{xy}}{E\left(I_{xx}I_{yy}-I_{xy}{}^2\right)} \tag{5}$$

where, I_{xx} and I_{yy} are the second moment of inertia with respect to x- and y-axis, respectively; I_{xy} represents the inertia product of cross section; E is the Young's modulus of elasticity; and the constants a_1, a_2, a_3, and a_4 are related to the section shape and expressed in a general form as:

$$a_1=\frac{I_{xx}\int\phi(x,y)ydA-I_{xy}\int\phi(x,y)xdA}{I_{xx}I_{yy}-I_{xy}{}^2} \tag{6}$$

$$a_2=\frac{I_{xx}\int\phi(x,y)xdA-I_{xy}\int\phi(x,y)ydA}{I_{xx}I_{yy}-I_{xy}{}^2} \tag{7}$$

$$a_3=-\frac{\mu L}{A}\left[C_xI_{xy}+\frac{1}{2}C_y\left(I_{xx}-I_{yy}\right)\right] \tag{8}$$

$$a_4=-\frac{\mu L}{A}\left[C_yI_{xy}+\frac{1}{2}C_x\left(I_{yy}-I_{xx}\right)\right] \tag{9}$$

The coordinates of shear center of the cross section are defined as:

$$x_{sc}=\frac{M_x}{V_y}=\frac{1}{V_y}\int\left(x\tau_{zy}\big|_{V_y=const,V_x=0}-y\tau_{zx}\big|_{V_y=const,V_x=0}\right)dA \tag{10}$$

$$y_{sc}=\frac{M_y}{V_x}=\frac{1}{V_x}\int\left(y\tau_{zx}\big|_{V_x=const,V_y=0}-x\tau_{zy}\big|_{V_x=const,V_y=0}\right)dA \tag{11}$$

In the above Eqs. (10) and (11), only applying V_y to the end of the cantilever beam can obtain x_{sc}, while only applying V_x to the end of the cantilever beam can obtain y_{sc}. Totally, two loading cases should be considered. It is noted that M_x is the torsion caused by V_y while M_y is the torsion caused by V_x.

According to the theory of elasticity mechanics, the normal and shear stresses can be written as:

$$\sigma_{zz}=-E(L-z)\left(xC_x+yC_y\right) \tag{12}$$

$$\tau_{zx}=G\left\{\frac{\partial\phi(x,y)}{\partial x}-\mu\left[\frac{1}{2}C_x\left(x^2-y^2\right)+xyC_y\right]\right\} \tag{13}$$

$$\tau_{zy}=G\left\{\frac{\partial\phi(x,y)}{\partial y}-\mu\left[xyC_x-\frac{1}{2}C_y\left(x^2-y^2\right)\right]\right\} \tag{14}$$

$$\sigma_{xx}=\sigma_{yy}=\tau_{xy}=0 \tag{15}$$

in which, G is the shear modulus of elasticity of the material.

Thus, the coordinates of shear center defined in Eqs. (10) and (11) can be rewritten as:

$$x_{sc}=\frac{G}{2V_y}\int\begin{bmatrix}2x\dfrac{\partial\phi(x,y)\big|_{V_y=const,V_x=0}}{\partial y}\\-2y\dfrac{\partial\phi(x,y)\big|_{V_y=const,V_x=0}}{\partial x}\\+\mu\left(C_yx-C_xy\right)\left(x^2+y^2\right)\end{bmatrix}dA \tag{16}$$

$$y_{sc}=-\frac{G}{2V_x}\int\begin{bmatrix}2x\dfrac{\partial\phi(x,y)\big|_{V_x=const,V_y=0}}{\partial y}\\-2y\dfrac{\partial\phi(x,y)\big|_{V_x=const,V_y=0}}{\partial x}\\+\mu\left(C_yx-C_xy\right)\left(x^2+y^2\right)\end{bmatrix}dA \tag{17}$$

The average deflections caused by shear forces weighted by the lateral displacements along the longitudinal z-axis of the cantilever beam are expressed as:

$$\bar{u}_s=\frac{1}{A}\int u_sdA \tag{18}$$

$$\bar{v}_s=\frac{1}{A}\int v_sdA \tag{19}$$

Further, the average shear deformation can be expressed as:

$$\frac{d\bar{u}_s}{dz}=\frac{\partial\left(\frac{1}{A}\int u_sdA\right)}{\partial z}=\frac{1}{A}\frac{\partial\left(\int u_sdA\right)}{\partial z} \tag{20}$$

$$\frac{d\bar{v}_s}{dz}=\frac{\partial\left(\frac{1}{A}\int v_sdA\right)}{\partial z}=\frac{1}{A}\frac{\partial\left(\int v_sdA\right)}{\partial z} \tag{21}$$

Substituting Eqs. (1) to (3) into Eqs. (20) and (21), it leads to:

$$\frac{d\bar{u}_s}{dz}=\frac{V_x}{GA_{xx}}+\frac{V_y}{GA_{xy}}=\frac{V_x}{GAk_{xx}}+\frac{V_y}{GAk_{xy}} \tag{22}$$

$$\frac{d\bar{v}_s}{dz}=\frac{V_x}{GA_{yx}}+\frac{V_y}{GA_{yy}}=\frac{V_x}{GAk_{yx}}+\frac{V_y}{GAk_{yy}} \tag{23}$$

In Eqs. (22) and (23), the term $V_i/\left(GAk_{ii}\right)$ represents the deflection along i-axis caused by shear force V_i, while the term $V_j/\left(GAk_{ij}\right)$ represents the deflection along i-axis caused by shear force V_j. Subscript i can be x or y. Totally, there are four shear correction factors, i.e., k_{xx}, k_{xy}, k_{yx}, and k_{yy} as given in Eqs. (24) to (26). Since the shear deformation along x-axis (or y-axis) is mainly caused by the shear force along x-axis (or y-axis), the hybrid shear correction factors k_{xy} and k_{yx} are rarely adopted in the practical structural analysis using beam-column model. Thus, only k_{xx} and k_{yy} are discussed in this paper.

$$k_{xx}=\frac{I_{xx}I_{yy}-I_{xy}{}^2}{\left\{\frac{GA}{V_x}\left[I_{xx}\int x\phi(x,y)\big|_{V_x=const,V_y=0}dA-I_{xy}\int y\phi(x,y)\big|_{V_x=const,V_y=0}dA\right]-q_1\right\}} \tag{24}$$

$$k_{xy}=k_{yx}=-\frac{4(1+\mu)}{\mu}\cdot\frac{\left(I_{xx}I_{yy}-I_{xy}^{\ 2}\right)}{I_{xy}\left(I_{yy}+I_{xx}\right)} \tag{25}$$

$$k_{yy}=\frac{I_{xx}I_{yy}-I_{xy}^{\ 2}}{\left\{\frac{GA}{V_y}\left[I_{yy}\int y\phi(x,y)\big|_{V_y=const,V_x=0}\,dA-I_{xy}\int x\phi(x,y)\big|_{V_y=const,V_x=0}\,dA\right]-q_2\right\}} \tag{26}$$

in which, q_1 and q_2 are the constants given by:

$$q_1=\frac{\mu}{4(1+\mu)}\left[I_{xx}\left(I_{yy}-I_{xx}\right)-2I_{xy}^{\ 2}\right] \tag{27}$$

$$q_2=\frac{\mu}{4(1+\mu)}\left[I_{yy}\left(I_{xx}-I_{yy}\right)-2I_{xy}^{\ 2}\right] \tag{28}$$

From Eqs. (24) and (26), the shear correction factors depended on the section properties (A, I_{xx}, I_{yy}, and I_{xy}), material properties (shear modulus of elasticity G and Poisson's ratio μ), and warping function $\phi(x,y)$. Thus, once the warping function $\phi(x,y)$ is known, the shear correction factors can be determined accordingly. This paper proposes a numerical method to determine the solution of the warping function $\phi(x,y)$.

2.3. Warping function for one-dimensional element

This Section introduces a finite element method to obtain the solution of warping function $\phi(x,y)$ as shown in Eqs. (24) and (26).

Based on the conventional fiber-based approach, a section can be represented by a number of area elements allowing for warping effect as shown in Fig. 2(a). The value of $\phi(x,y)$ at each node of the plane element is denoted as ϕ_i. Thus, the $\phi(x,y)$ at the any location of the element can be interpolated by:

$$\phi=\sum_{i=1}^{n}N_i(\xi,\eta)\phi_i \tag{29}$$

Using theory of iso-parametric element, the coordinates of the element can be expressed as:

$$x=\sum_{i=1}^{n}N_i(\xi,\eta)x_i \tag{30}$$

$$y=\sum_{i=1}^{n}N_i(\xi,\eta)y_i \tag{31}$$

where, ξ and η are the natural coordinates as seen in Fig. 3(a); n is the number of nodes of the element; and $N_i(\xi,\eta)$ is the shape function which will be introduced in the followings.

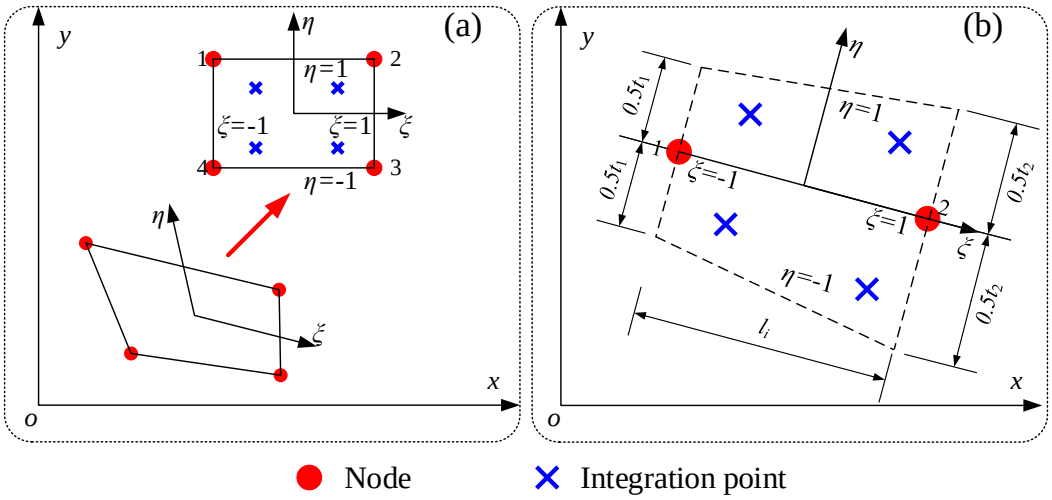

Fig. 4 Iso-parametric elements: (a) Conventional plane warping area element; and (b) Proposed one-dimensional warping element

In this paper, a one-dimensional warping element as shown in Fig. 4(b) is proposed to achieve modelling simplicity and computational efficiency. A thin-walled section can be represented by several two-node segments modelled by the proposed element. For comparison and verification purposes, a conventional plane warping area element with four nodes as shown in Fig. 4(a) is also developed here.

In the proposed element, the coordinates of the two nodes are denoted as (x_1, y_1) and (x_2, y_2). For thin-walled sections with non-uniform thickness, the thickness of the thin-walled segment at the first end is assumed as t_1 while the other end is t_2. As the linear form of $N_i(\xi,\eta)$ is adopted, the coordinates at any location in the one-dimensional warping element can be expressed as:

$$\begin{aligned}x&=\sum_{i=1}^{2}N_i(\xi)x_i+\sum_{i=1}^{2}H_i(\xi,\eta)t_i\sin\theta_i\\&=\frac{1-\xi}{2}x_1+\frac{1+\xi}{2}x_2-\frac{1-\xi}{2}\frac{\eta}{2}t_1\sin\theta_i-\frac{1+\xi}{2}\frac{\eta}{2}t_2\sin\theta_i\end{aligned} \tag{32}$$

$$\begin{aligned}y&=\sum_{i=1}^{2}N_i(\xi)y_i+\sum_{i=1}^{2}H_i(\xi,\eta)t_i\cos\theta_i\\&=\frac{1-\xi}{2}y_1+\frac{1+\xi}{2}y_2+\frac{1-\xi}{2}\frac{\eta}{2}t_1\cos\theta_i+\frac{1+\xi}{2}\frac{\eta}{2}t_2\cos\theta_i\end{aligned} \tag{33}$$

Note that $N_i(\xi)$ and $H_i(\xi,\eta)$ are two special forms of $N_i(\xi,\eta)$ for the proposed element, θ_i is angle of the i^{th} one-dimensional warping element.

Due to the change of the shear stress along the plate thickness is ignored, the warping displacement not related with the thickness term can be expressed as:

$$\phi=\sum_{i=1}^{2}N_i(\xi)\phi_i=\frac{1-\xi}{2}\phi_1+\frac{1+\xi}{2}\phi_2 \tag{34}$$

By differentiating Eq. (34), it gives:

$$\begin{cases}\dfrac{\partial\phi(x,y)}{\partial x}=\displaystyle\sum_{i=1}^{2}\frac{\partial N_i(\xi)}{\partial x}\phi_i=\frac{(x_1-x_2)}{l_i}\phi_1+\frac{(-x_1+x_2)}{l_i}\phi_2\\[2ex]\dfrac{\partial\phi(x,y)}{\partial y}=\displaystyle\sum_{i=1}^{2}\frac{\partial N_i(\xi)}{\partial y}\phi_i=\frac{(y_1-y_2)}{l_i}\phi_1+\frac{(-y_1+y_2)}{l_i}\phi_2\end{cases} \tag{35}$$

$$\sin\theta_i=\frac{y_2-y_1}{l_i},\quad\cos\theta_i=\frac{x_2-x_1}{l_i},\quad l_i=\sqrt{(x_2-x_1)^2+(y_2-y_1)^2} \tag{36}$$

2.4. Stiffness matrix and load vector

The energy method is adopted here to derive the element stiffness matrix. From Section 2.3, the basic unknowns of the section are the warping displacements at two ends, i.e. $\boldsymbol{\Delta}_{si}=\{\phi_1,\ \phi_2\}^T$. The total potential energy of the proposed element is expressed as:

$$\Pi_{si} = U_{si} - W_{si} \tag{37}$$

in which, U_{si} represents the strain energy and W_{si} is the work done by external loads. They are given by:

$$\begin{aligned} U_{si} &= \frac{1}{2}\int\left(\sigma_{zz}\varepsilon_{zz} + \tau_{zy}\gamma_{zy} + \tau_{zx}\gamma_{zx}\right)dV_i \\ &= \frac{1}{6}GL^3\int\left(C_x x + C_y y\right)^2 dA_i + \frac{1}{2}GL^3\int\left[\left(\frac{\partial\phi(x,y)}{\partial x} - C_1\right)^2 + \left(\frac{\partial\phi(x,y)}{\partial y} - C_2\right)^2\right]dA_i \end{aligned} \tag{38}$$

$$\begin{aligned} W_{si} &= V_{x,i}\bar{u}\big|_{z=L} + V_{y,i}\bar{v}\big|_{z=L} = V_{x,i}\left(\frac{1}{3}C_x L^3 + a_2 L + a_4\right) + V_{y,i}\left(\frac{1}{3}C_y L^3 + a_1 L + a_3\right) \\ &= V_x\frac{\int dA_i}{A}\left(\frac{1}{3}C_x L^3 + a_2 L + a_4\right) + V_y\frac{\int dA_i}{A}\left(\frac{1}{3}C_y L^3 + a_1 L + a_3\right) \end{aligned} \tag{39}$$

where, A_i is the area of the i^{th} element. The constants C_1 and C_2 are given by:

$$C_1 = \mu\left[\frac{1}{2}C_x\left(x^2 - y^2\right) + xyC_y\right] \tag{40}$$

$$C_2 = \mu\left[\frac{1}{2}C_y\left(y^2 - x^2\right) + xyC_x\right] \tag{41}$$

By using the principle of stationary potential energy, we have:

$$\frac{\partial\Pi_{si}}{\partial\phi_i} = 0,\ i = 1,\ 2 \tag{42}$$

Thus, the element stiffness matrix $\mathbf{k_e}$ can be obtained as:

$$\mathbf{k_e} = \left[k_{ij}\right] = \left[\frac{\partial^2\Pi_{si}}{\partial\phi_i\partial\phi_j}\right] = \left[G\int_{-1}^{1}\int_{-1}^{1}\left(\frac{\partial N_i}{\partial x}\frac{\partial N_j}{\partial x} + \frac{\partial N_i}{\partial y}\frac{\partial N_j}{\partial y}\right)\left|\mathbf{J_F}\right|d\xi d\eta\right] \tag{43}$$
$$\left(i = 1,2 \text{ and } j = 1,2\right)$$

where, $\mathbf{J_F}$ is the Jacobi matrix which is calculated as:

$$\begin{aligned} J_F &= \begin{bmatrix} \frac{\partial x}{\partial\xi} & \frac{\partial y}{\partial\xi} \\ \frac{\partial x}{\partial\eta} & \frac{\partial y}{\partial\eta} \end{bmatrix} \\ &= \begin{bmatrix} \frac{x_2}{2} - \frac{x_1}{2} + \eta t_1\frac{\sin\theta_i}{4} - \eta t_2\frac{\sin\theta_i}{4} & \frac{y_2}{2} - \frac{y_1}{2} - \eta t_1\frac{\cos\theta_i}{4} + \eta t_2\frac{\cos\theta_i}{4} \\ \left(-\frac{1-\xi}{4}t_1 - \frac{1+\xi}{4}t_2\right)\sin\theta_i & \left(\frac{1-\xi}{4}t_1 + \frac{1+\xi}{4}t_2\right)\cos\theta_i \end{bmatrix} \end{aligned} \tag{44}$$

Note that the well-known Gauss-Legendre 2×2 Integral scheme as listed in Table 1 has been adopted in this paper to determine the element stiffness matrix. It should be pointed out that the proposed warping element allowing for non-uniform thickness has not been reported in previous study.

Table 1
Gauss-Legendre 2×2 Integration Scheme

Integral variable	Integration point	Weight
ξ	+0.774596692	1.0
	-0.774596692	1.0
η	+0.774596692	1.0
	-0.774596692	1.0

Then, the load vector $\mathbf{f_{es}}$ of the element is expressed as:

$$\begin{aligned} \mathbf{f_{es}} &= \left\{f_{esi}\right\} = \left\{-\frac{\partial\Pi_{si}}{\partial\phi_i} + \sum_{i=1}^{2}k_{ij}\phi_j\right\} \\ &= \left\{G\int_{-1}^{1}\int_{-1}^{1}\left(C_1\frac{\partial N_i}{\partial x} + C_2\frac{\partial N_i}{\partial y}\right)\left|\mathbf{J_F}\right|d\xi d\eta + E\int_{-1}^{1}\int_{-1}^{1}N_i\left(xC_x + yC_y\right)\left|\mathbf{J_F}\right|d\xi d\eta\right\} \\ &\left(i = 1,2\right) \end{aligned} \tag{45}$$

The system stiffness matrix $\mathbf{K}$ can be formed by assembling all element stiffness $\mathbf{k_e}$ while the total load vector $\mathbf{F_s}$ is formed by all element load vector $\mathbf{f_{es}}$. Finally, the equilibrium equations of the section can be written as:

$$\mathbf{K\Delta_s} = \mathbf{F_s} \tag{46}$$

in which, $\mathbf{\Delta_s} = \left\{\phi_{s1},\ \phi_{s2},\ ...,\ \phi_{sm}\right\}^T$ is the warping displacements of the section represented by several proposed elements, and subscript m is the number of nodes of the section. Thus, the conventional linear solvers can be used to solve the system of equations in Eq. (46). After that, the shear correction factors can be calculated by Eqs. (24) and (26) using the warping displacements $\mathbf{\Delta_s}$.

For isotropic material, it has $G=E/[2(1+\mu)]$. From Eqs. (43) and (45), the material properties such as Young's modulus E and shear modulus G can be eliminated in Eq. (46) when only one isotropic material is adopted in the section concerned. Thus, the warping displacements $\mathbf{\Delta_s}$ will be affected by Poisson's ratio only in regard to material properties.

3. Modelling of built-up thin-walled sections

Nowadays, the built-up sections composed of several single sections such as angles and channels connected with fasteners such as screws, bolts, and clinches have been extensively used for economic design and fast construction. It is clear that the section properties such as A, I_{xx}, I_{yy}, and I_{xy} of the built-up section will be not less than the summation of the individual sections. Normally, the second moment of inertia I_{xx} and I_{yy} of the built-up section will be significantly increased due to composite action. Note that there is few research on the shear correction factors of built-up sections. Because the numerical method proposed in Section 0 is only for the cross sections in a continuous domain, an additional procedure is introduced in this Section so that the built-up sections with several discontinuous domains can be converted to a single continuous one.

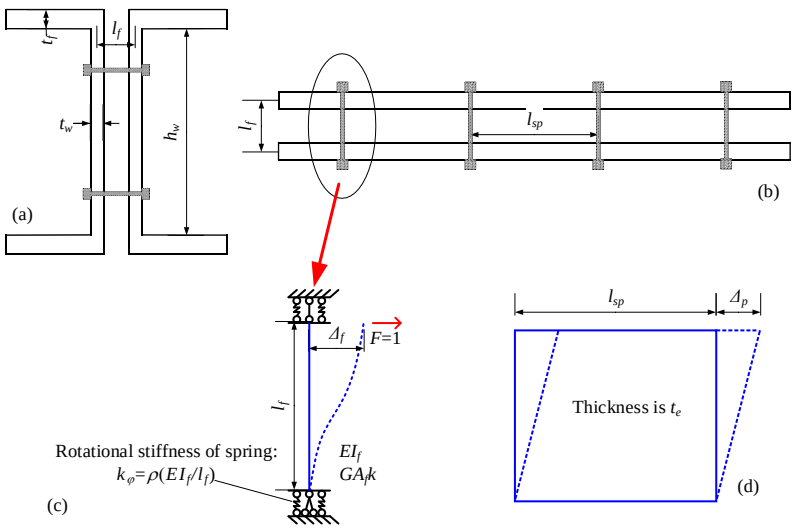

Fig. 5 Model for calculation of equivalent thickness of built-up section: (a) Section view; (b) Plan view; (c) Modeling of the fastener; and (d) Equivalent plate for the fastener

In this paper, an analytical method is proposed to convert the discrete fasteners to plates connecting the individual parts, leading that a built-up section can be treated as a single section with continuous domain. By using this method, an equivalent plate thickness should be determined for the plate representing the associated fastener. A double-channel section as shown in Fig. 5(a) and (b). is adopted here to demonstrate the proposed analytical method. The discrete fastener is treated as a beam with two ends constrained by springs as shown in Fig. 5(c). The rotational stiffness of the spring is expressed as:

$$k_\varphi = \rho \frac{EI_f}{l_f} \tag{47}$$

where, ρ is a rigidity coefficient; E is Young's Modulus; I_f is the second moment of inertia of the fastener; l_f is the length. In Fig. 5, A_f is the sectional-area of the fastener; l_{sp} is the longitudinal spacing between the adjacent fasteners, t_f is the thickness of the flange, t_w is the thickness of the connected web, and h_w is the height of the web.

Applying a virtual unit force F at one end of the fastener as indicated in Fig. 5(c), the energy of the fastener can be written as:

$$\begin{aligned} U_f &= \frac{l_f^3}{24EI} + \frac{l_f}{2GA_f k_f} + 2\times\frac{1}{2}\times\frac{l_f}{2}\times\frac{l_f}{2k_\varphi} \\ &= \frac{l_f^3}{24EI_f} + \frac{l_f}{2GA_f k_f} + \frac{l_f^3}{4\rho EI_f} \end{aligned} \tag{48}$$

where, k_f is the shear correction factors of the solid section of the fastener. For circular section, k_f is taken as 0.9.

The shear strain of the equivalent steel plate is expressed as:

$$\gamma = \frac{F}{Gl_{sp}t_e} \tag{49}$$

where, t_e is the thickness of the equivalent plate to be determined. The shear strain energy of the plate can be written as:

$$U_p = \frac{1}{2}G\gamma^2 l_f l_{sp} t_e = \frac{1}{2}G\left(\frac{F}{Gl_{sp}t_e}\right)^2 l_f l_{sp} t_e = \frac{l_f}{2Gl_{sp}t_e} \tag{50}$$

According to the principle of conservation of energy, U_p should be equal to U_f. Thus, the equivalent plate thickness t_e can be derived as:

$$t_e = \frac{1}{l_{sp}\left[\dfrac{l_f^2}{24(1+\mu)I_f} + \dfrac{1}{A_f k_f} + \dfrac{l_f^2}{4\rho(1+\mu)I_f}\right]} \tag{51}$$

For fully fixed end condition, i.e. $\rho\to\infty$, the upper bound of t_e can be obtained from Eq. (47):

$$t_{e,\max} = \frac{1}{l_{sp}\left[\dfrac{l_f^2}{24(1+\mu)I_f} + \dfrac{1}{A_f k_f}\right]} \tag{52}$$

As the stiffness of the constraint spring does not equal to zero, a lower bound of t_e can also be derived. As shown in Fig. 5, the fastener is subjected to the constraints provided by the web of the channel. It is noted that the influences of the flange of the channel to the constraint spring are ignored. Thus, a simple model as shown in Fig. 6 is proposed for representation of the lath cut from the web. The stiffness of the lath per unit width can be written as:

$$D_l = \frac{Et_w^3}{12(1-\mu^2)} \tag{53}$$

Therefore, the corresponding rigidity coefficient ρ of the spring is expressed as:

$$\begin{aligned} \rho &= k_\varphi \frac{l_f}{EI_f} = \frac{2M_1}{\theta'}\frac{l_f}{EI_f} = \frac{4D_l\left(\dfrac{h_w}{N_r}\right)}{l_{sp}}\frac{l_f}{EI_f} \\ &= \frac{Et_w^3}{12(1-\mu^2)}\frac{4}{l_{sp}}\frac{h_w}{N_r}\frac{l_f}{EI_f} = \frac{t_w^3 h_w l_f}{3(1-\mu^2)l_{sp}N_r I_f} \end{aligned} \tag{54}$$

where, N_r is the number of fasteners at a section, h_w/N_r represents the width of the lath cut from the web for supporting one fastener. From Eq. (50), the lower bound of t_e can be obtained as:

$$t_{e,\min} = \frac{1}{l_{sp}\left[\dfrac{l_f^2}{24(1+\mu)I_f} + \dfrac{1}{A_f k_f} + \dfrac{3(1-\mu)l_f l_{sp} N_r}{4t_w^3 h_w}\right]} \tag{55}$$

As t_e is relatively small and mainly for maintaining the domain continuity of the cross section, its contribution on section properties such as A, I_{xx}, I_{yy}, and I_{xy} is ignored here. However, it may influence the shear flow and then shear correction factors of the built-up section. The upper bound $t_{e,\max}$ provides the maximum shear correction factors, while the lower bound $t_{e,\min}$ gives the minimum shear correction factors. The verification and discussion of Eqs. (48) to (55) will be illustrated in a worked example in Section 5.6.

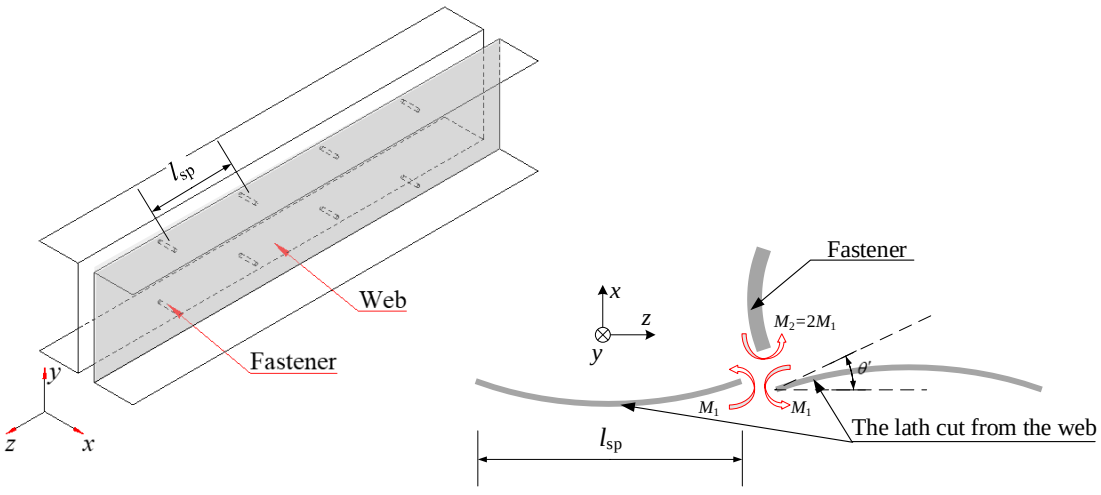

Fig. 6 The lath cut from the web and the constraint actions

4. Numerical implementation

From Eqs. (24) and (26), the basic section properties such as A, I_{xx}, I_{yy}, and I_{xy} should be calculated before determining the shear correction factors. These basic section properties can be easily obtained by summing A_i, $I_{i,xx}$, $I_{i,yy}$, and $I_{i,xy}$

of all elements. The subscript i means the contributions of the i^{th} one-dimensional warping element to the section properties. More specifically, they can be computed as:

$$A_i = \int l_i dt = \frac{l_i (t_{i1} + t_{i2})}{2} \tag{56}$$

$$I_{i,xx} = \int y^2 dA_i = \frac{1}{3} A_i \left(y_{i1}^{\ 2} + y_{i1} y_{i2} + y_{i2}^{\ 2} \right) + \frac{1}{48} A_i \left(t_{i1} + t_{i2} \right)^2 \cos \theta_i^2 \tag{57}$$

$$I_{i,yy} = \int x^2 dA_i = \frac{1}{3} A_i \left(x_{i1}^{\ 2} + x_{i1} x_{i2} + x_{i2}^{\ 2} \right) + \frac{1}{48} A_i \left(t_{i1} + t_{i2} \right)^2 \sin \theta_i^2 \tag{58}$$

$$I_{i,xy} = \int xy dA_i = \frac{1}{6} A_i \left(2x_{i1} y_{i1} + x_{i1} y_{i2} + x_{i2} y_{i1} + 2x_{i2} y_{i2} \right) - \frac{1}{48} A_i \left(t_{i1} + t_{i2} \right)^2 \sin \theta_i \cos \theta_i \tag{59}$$

where, (x_{i1}, y_{i1}) and (x_{i2}, y_{i2}) are the coordinates of the element two ends by referring to the centroid.

Fig. 7 shows the flowchart of the procedure to find the shear center and the shear correction factors based on the proposed method introduced in Section 2 and 3. The method is implemented in the program NIDA (2021). The verification examples in the next Section are then prepared by using the program NIDA.

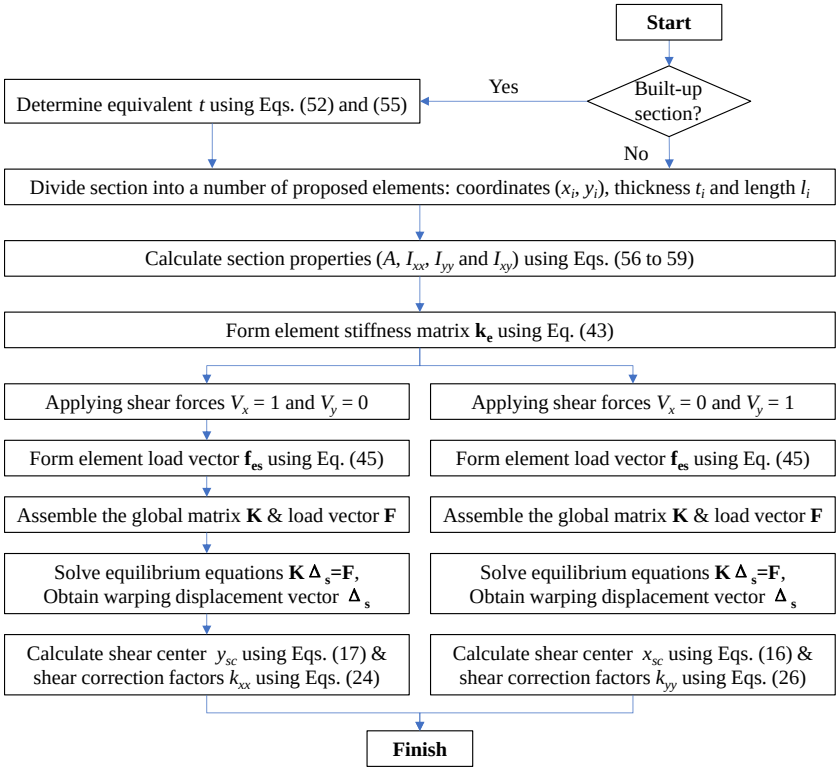

Fig. 7 Flowchart for calculation of shear correction factors

5. Verification examples

To validate the accuracy and the efficiency of the proposed method, six examples are investigated here with consideration of single sections in regular shape, open and closed thin-walled sections, complex sections with non-uniform thickness, built-up sections. The results predicted by the proposed element will be verified against the analytical solution, conventional warping area element method and the section analysis in commercial software ANSYS based on fiber section approach. Further, an example is provided at the end to demonstrate the influence of shear correction factors and the application of the proposed method in conjunction with the Direct Analysis Method.

5.1. Example 1 – Rectangular and trapezoidal sections

The rectangular sections are the simplest and widely used cross sections, as shown in Fig. 8. The analytical solution for the shear correction factors of rectangular sections with consideration of Poisson effect has been well-developed by [21]Herrmann (1965). To verify the performance of the proposed element in sections with non-uniform thickness, the trapezoidal sections are also studied here.

In this example, the rectangular sections with different height-to-width (h/b) ratios equal to 10, 5, 2, 1, 0.5 and 0.25 are studied. The rectangular section is divided into a number of the proposed 1D warping elements along the height. To study the mesh sensitivity, the Poisson's ratio is assumed as 0 and the results are shown in Fig. 9. It is observed that the shear correction factors vary with the increase of the number of elements. Clearly, 20 elements per segment can lead to convergent results for the shear correction factors. Also, the rectangular sections with different h/b ratios show the same trend. Thus, it is recommended at least 20 elements should be used for each segment of the thin-wall sections to get an accurate result.

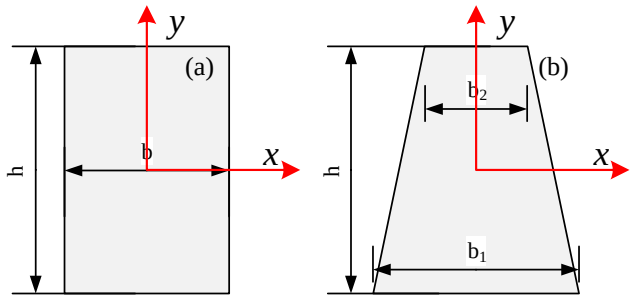

Fig. 8 Simple plate sections: (a) Rectangular; and (b) Trapezoidal

Further, the influence of Poisson effect is studied to investigate the accuracy of the present method. An analytical formula including Poisson's ratio proposed by Leonard[23] in 1965 is adopted here for the validation. The shear correction factor along one axis of the rectangular section can be calculated by:

$$k = \frac{10(1+\mu)}{12+11\mu} \tag{60}$$

To study the Poisson effect on shear correct factors, different Poisson's ratios (i.e. 0, 0.2, 0.25, 0.3, 0.5) in related commonly used materials in building and bridge structures are assumed for the above rectangular sections. The shear correction factors predicted by the proposed method are listed in Table 2 against the results obtained by the analytical solution from Eq. (60) and the element Plane82 in software ANSYS. It can be seen that the results from present study agree well with the analytical solution. As the change of Poisson's ratio does not affect the result from ANSYS, it can be concluded that the section analysis method in ANSYS cannot consider the Poisson effect.

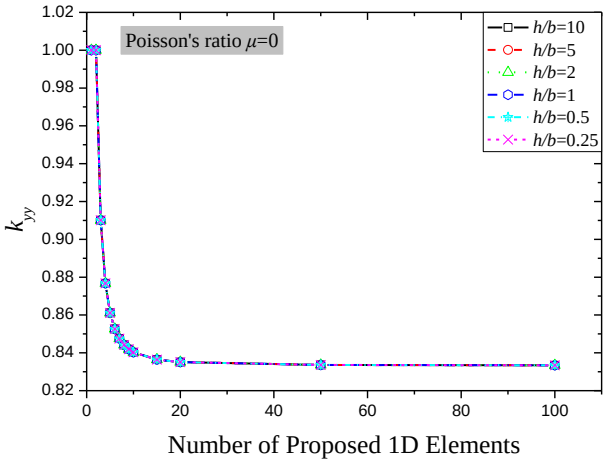

Fig. 9 Mesh sensitivity study for rectangular section

Table 2
Shear correction factors of rectangular sections

Poisson's ratio	① Analytical	② ANSYS	③ Present	Diff (③-①)/① (%)	Diff (③-②)/② (%)
0	0.8333	0.8333	0.8334	0.012	0.012
0.20	0.8451	0.8333	0.8451	0	1.416
0.25	0.8475	0.8333	0.8475	0	1.704
0.30	0.8497	0.8333	0.8497	0	1.968
0.50	0.8571	0.8333	0.8572	0.012	2.868

To study the sections with non-uniform thickness, the trapezoidal sections as shown in Fig. 7(b) with h/b_1 equal to 1, 2, 3 and 4 are also investigated. For simplicity, the h/b_2 ratios for different h/b_1 ratios are kept as 10. The results from present study are given in Table 3 against the results from traditional warping area element method and ANSYS. It can be seen that the proposed method can provide accurate shear correction factors when $h/b_1 \geq 2$.

Table 3
Shear correction factors of trapezoidal sections

h/b_1	①Warping area element	② ANSYS	③Present	Diff (③-①)/① (%)	Diff (③-②)/② (%)
1	0.7849	0.7818	0.8361	6.523	6.946
2	0.8313	0.8197	0.8425	1.347	2.782
3	0.8411	0.8270	0.8437	0.309	2.019
4	0.8441	0.8298	0.8458	0.201	1.928

5.2. Example 2 – Typical open sections

This example investigates the shear center and shear correction factors of several commonly used steel open sections such as unequal I-section, Tee, angle, channel and z sections by the proposed numerical method. To study the influence of plate thickness, the section classification according to Hong Kong Steel Code (CoPSC 2011) as shown in Table 4 is adopted. Poisson's ratio is taken as 0 and 0.3 for all sections. The value of 0.3 represents steel material. For comparison purpose, the results from ANSYS using Plane82 element are also presented. The shear correction factors and shear centers obtained from the present method are listed in Table 5 to Table 9 against the results from ANSYS.

It can be concluded that as the plate thickness decreases, the difference tends to be smaller. It may be caused not only by the assumption of ignoring the nonuniform shear stress along the plate thickness but also the overlapped effect (Fig. 11) by using the one-dimensional warping element. The overall agreement between the proposed method and ANSYS can be observed within 10% difference which meets the requirements of engineering. Also, since ANSYS cannot consider the Poisson effect, the results predicted by the presented method with Poisson's ratio = 0 agree well with ANSYS, especially for Tee, Angle and Zee sections.

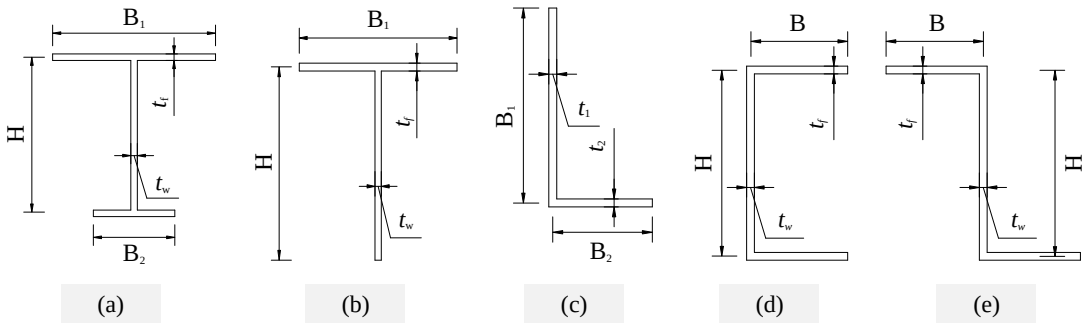

Fig. 10 Open sections: (a) Unequal I; (b) Tee; (c) Angle; (d) Channel; and (e) Z-shape

Table 4
The *b/t* ratios for the section classification in CoPSC 2011

Ratio	Class 1 Plastic	Class 2 Compact	Class 3 Semi-compact	Class 4 Slender
b/t	8	9	13	>13

Table 5
Shear center and shear correction factors of Unequal I-section

$B_1 \times B_2 \times H \times t_f \times t_w$(m)	Parameter	①ANSYS (μ=0)	②Present (μ=0)	③Present (μ=0.3)	Diff (②-①)/① (%)	Diff (③-①)/① (%)
Class 1: 0.4×0.2×0.4×0.05×0.05	y_{sc} (m)	0.1100	0.1140	0.1208	3.611	9.818
	k_{xx}	0.4577	0.4205	0.4205	-8.118	-8.128
	k_{yy}	0.4098	0.3660	0.3667	-10.691	-10.517

Class 3: 0.4×0.2×0.4×0.02×0.02	y_{sc} (m)	0.1142	0.1153	0.1222	0.963	7.005
	k_{xx}	0.4258	0.4109	0.4110	-3.495	-3.476
	k_{yy}	0.3792	0.3632	0.3638	-4.210	-4.061
Class 4: 0.4×0.2×0.4×0.01×0.01	y_{sc} (m)	0.1150	0.1155	0.1224	0.427	6.435
	k_{xx}	0.4170	0.4096	0.4097	-1.786	-1.751
	k_{yy}	0.3706	0.3628	0.3634	-2.093	-1.943

Table 6
Shear center and shear correction factors of Tee section

B×H×t_f×t_w(m)	Parameter	①ANSYS (μ=0)	②Present (μ=0)	③Present (μ=0.3)	Diff (②-①)/① (%)	Diff (③-①)/① (%)
Class 1: 0.4×0.4×0.05×0.05	y_{sc} (m)	0.0975	0.0985	0.0886	0.986	-9.128
	k_{xx}	0.459	0.4298	0.4178	-6.362	-8.976
	k_{yy}	0.4355	0.3980	0.3943	-8.606	-9.460
Class 3: 0.4×0.4×0.02×0.02	y_{sc} (m)	0.0975	0.0998	0.0886	2.308	-9.128
	k_{xx}	0.459	0.4188	0.4178	-8.768	-8.976
	k_{yy}	0.4355	0.3939	0.3943	-9.559	-9.460
Class 4: 0.4×0.4×0.01×0.01	y_{sc} (m)	0.1004	0.0999	0.0899	-0.461	-10.458
	k_{xx}	0.423	0.4181	0.4055	-1.169	-4.137
	k_{yy}	0.4002	0.3942	0.3895	-1.490	-2.674

Table 7
Shear center and shear correction factors of Angle section

B_1×B_2×t_1×t_2(m)	Parameter	①ANSYS (μ=0)	②Present (μ=0)	③Present (μ=0.3)	Diff (②-①)/① (%)	Diff (③-①)/① (%)
Class 1: 0.25×0.25×0.05×0.05	x_{sc} (m)	-0.0591	-0.0619	-0.0624	4.706	5.584
	y_{sc} (m)	-0.0591	-0.0619	-0.0624	4.706	5.584
	k_{xx}	0.4684	0.4397	0.4349	-6.124	-7.152
	k_{yy}	0.4684	0.4397	0.4349	-6.124	-7.152
Class 3: 0.25×0.25×0.02×0.02	x_{sc} (m)	-0.062	-0.0624	-0.0629	0.645	1.452
	y_{sc} (m)	-0.062	-0.0624	-0.0629	0.645	1.452
	k_{xx}	0.4294	0.4222	0.4174	-1.682	-2.795
	k_{yy}	0.4294	0.4222	0.4174	-1.682	-2.795
Class 4: 0.25×0.25×0.01×0.01	x_{sc} (m)	-0.0624	-0.0625	-0.0629	0.120	0.801
	y_{sc} (m)	-0.0624	-0.0625	-0.0629	0.120	0.801
	k_{xx}	0.4217	0.4197	0.4149	-0.482	-1.613
	k_{yy}	0.4217	0.4197	0.4149	-0.482	-1.613

Table 8
Shear center and shear correction factors of Channel section

B×H×t_f×t_w(m)	Parameter	①ANSYS (μ=0)	②Present (μ=0)	③Present (μ=0.3)	Diff (②-①)/① (%)	Diff (③-①)/① (%)
Class 1: 0.3×0.5×0.05×0.05	x_{sc} (m)	-0.1947	-0.1987	-0.2025	2.050	4.006
	k_{xx}	0.3974	0.3668	0.3962	-7.710	-0.302
	k_{yy}	0.3837	0.3642	0.3674	-5.070	-4.248
Class 3: 0.3×0.5×0.03×0.03	x_{sc} (m)	-0.1976	-0.1990	-0.2028	0.720	2.632
	k_{xx}	0.3789	0.3622	0.3914	-4.402	3.299
	k_{yy}	0.3738	0.3630	0.3661	-2.881	-2.060
Class 4: 0.3×0.5×0.01×0.01	x_{sc} (m)	-0.199	-0.1992	-0.203	0.095	2.010
	k_{xx}	0.365	0.3600	0.389	-1.380	6.575
	k_{yy}	0.3658	0.3624	0.3655	-0.922	-0.082

Table 9
Shear correction factors of Z-shape section

B×H×t_f×t_w(m)	Parameter	①ANSYS (μ=0)	②Present (μ=0)	③Present (μ=0.3)	Diff (②-①)/① (%)	Diff (③-①)/① (%)
Class 1: 0.3×0.5×0.06×0.06	k_{xx}	0.4862	0.4567	0.5077	-6.060	4.422
	k_{yy}	0.4392	0.4221	0.4019	-3.897	-8.493

Class 3: 0.3×0.5×0.03×0.03	k_{xx}	0.4649	0.4485	0.4992	-3.535	7.378
	k_{yy}	0.4281	0.4185	0.3985	-2.233	-6.914
Class 4: 0.3×0.5×0.015×0.015	k_{xx}	0.4503	0.4485	0.4949	-0.407	9.905
	k_{yy}	0.4206	0.4185	0.3969	-0.490	-5.635

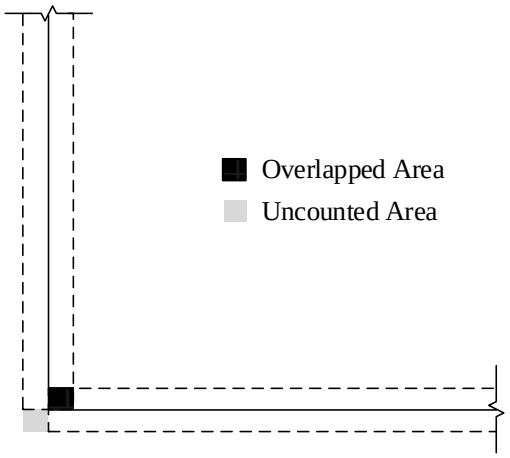

Fig. 11 The overlapped effect induced from the one-dimensional element modelling

5.3. Example 3 – Typical closed sections

This example investigates the shear center and shear correction factors of several commonly used steel close sections such as rectangular, circular and elliptic hollow sections as illustrated in Fig. 12. Poisson's ratio is taken as 0 and 0.3 for all sections. The value of 0.3 represents steel material. Three different plate thicknesses are studied for each section shape. For circular and elliptic hollow sections, several straight elements are used instead of curved element. For comparison purpose, the results from ANSYS using Plane82 element are also presented. The shear correction factors and shear centers obtained from the present method are listed in Table 10 to Table 12 against the results from ANSYS.

It can be concluded that as the plate thickness decreases, the difference tends to be smaller. It may be caused not only by the assumption of ignoring the nonuniform shear stress along the plate thickness but also the overlapped effect by using the one-dimensional warping element. The overall agreement between the proposed method by assuming Poisson's ratio as 0 and ANSYS can be observed within 5% difference which meets the engineering requirements. It also indicates that a relatively large difference may occur if ignoring the Poisson's ratio. Thus, ANSYS may not provide accurate shear correction factors for some cross sections.

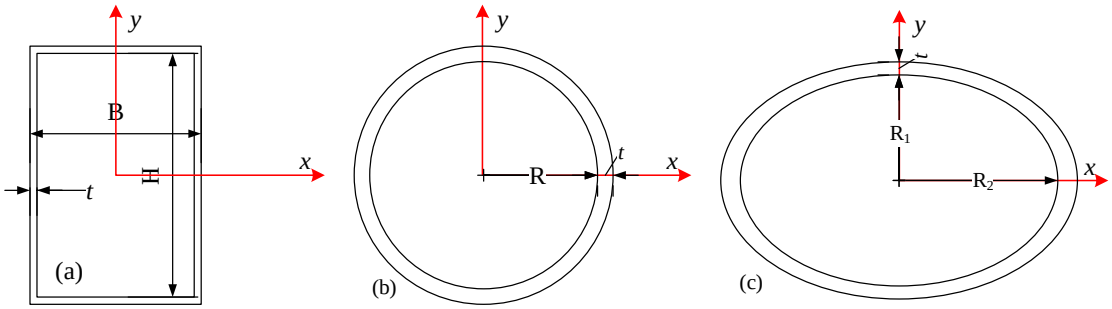

Fig. 12 Hollow sections: (a) Rectangular; (b) Circular; and (c) Elliptic

Table 10
Shear correction factors of rectangular hollow sections

B×H×*t*(m)	Parameter	①ANSYS (μ=0)	②Present (μ=0)	③Present (μ=0.3)	Diff (②-①)/①(%)	Diff (③-①)/①(%)
0.8×0.4×0.02	k_{xx}	0.2289	0.2235	0.2416	-2.377	5.548
	k_{yy}	0.6158	0.6107	0.6278	-0.834	1.949
0.8×0.4×0.008	k_{xx}	0.2255	0.2232	0.2413	-1.024	7.007
	k_{yy}	0.6127	0.6105	0.6277	-0.353	2.448
0.8×0.4×0.005	k_{xx}	0.2245	0.2232	0.2412	-0.597	7.439
	k_{yy}	0.6118	0.6105	0.6277	-0.209	2.599

Table 11
Shear correction factors of circular hollow sections

R×*t* (m)	Parameter	①ANSYS (μ=0)	②Present (μ=0)	③Present (μ=0.3)	Diff (②-①)/①(%)	Diff (③-①)/①(%)
0.2×0.02	k_{xx}	0.5023	0.5009	0.5316	-0.274	5.833
	k_{yy}	0.5023	0.5009	0.5316	-0.274	5.833
0.2×0.008	k_{xx}	0.5004	0.5001	0.5308	-0.052	6.075
	k_{yy}	0.5004	0.5001	0.5308	-0.052	6.075
0.2×0.002	k_{xx}	0.5	0.5000	0.5306	0.002	6.120
	k_{yy}	0.5	0.5000	0.5306	0.002	6.120

Table 12
Shear correction factors of elliptic hollow sections

$R_1 \times R_2 \times t$ (m)	Parameter	①ANSYS (μ=0)	②Present (μ=0)	③Present (μ=0.3)	Diff (②-①)/①(%)	Diff (③-①)/①(%)
0.4×0.2×0.02	k_{xx}	0.7131	0.7107	0.7359	-0.331	3.197
	k_{yy}	0.249	0.2476	0.2721	-0.559	9.277
0.4×0.2×0.008	k_{xx}	0.709	0.7101	0.7353	0.159	3.709
	k_{yy}	0.2458	0.2458	0.2701	0.020	9.886
0.4×0.2×0.002	k_{xx}	0.7187	0.7100	0.7351	-1.208	2.282
	k_{yy}	0.2335	0.2455	0.2698	5.154	15.546

5.4. Example 4 – Large stiffened box girder section

This example illustrates the accuracy of the presented one-dimensional warping element method in calculating the shear correction factors of large stiffened thin-walled steel box sections which is widely used in the bridge structures. Compared with the overall dimensions of the section, the plate thickness is much small. It causes high-density mesh when using the traditional warping area element method for this kind of sections.

In this paper, a stiffened steel box section as shown in Fig. 13 is studied, which is extensively adopted as the main girder in the large-span cable-supported bridges. Generally, many stiffeners are required to prevent local plate buckling and to achieve an economic design without use of thick plate. Two types of stiffeners are used in this box section, i.e. the closed U-ribs for flanges and flat-bar ribs for webs. Poisson's ratio is taken as 0 and 0.3. The shear center and shear correction factors from present study are shown in Table 13 against the results from traditional warping area element method allowing Poisson effect while ANSYS cannot consider this effect. It can be seen that the results from present study agree well with the warping area element method.

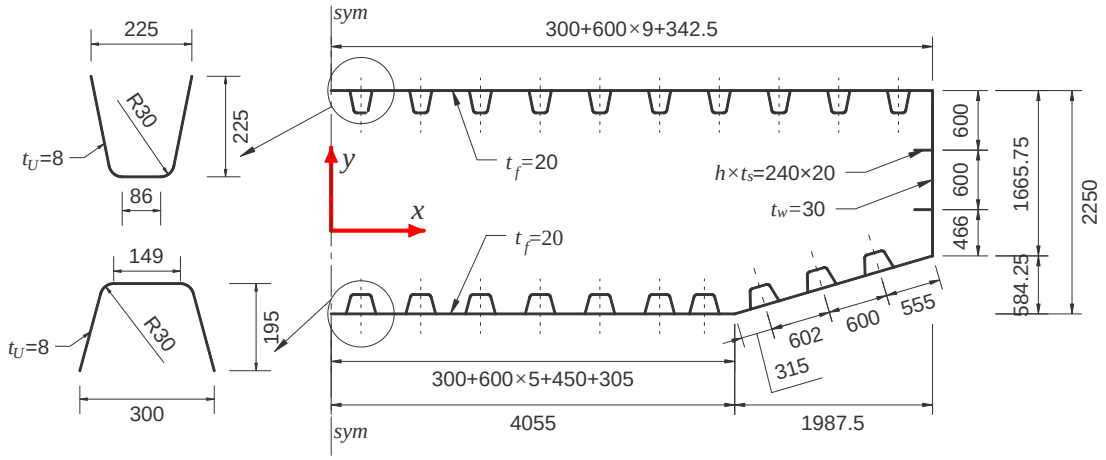

Fig. 13 Layout and dimensions of stiffened steel box section (unit: mm)

Table 13
Shear center and shear correction factors of stiffened steel box section

Parameter	①ANSYS (μ=0)	②Present (μ=0)	Diff (②-①)/①(%)	③Warping area element (μ=0.3)	④Present (μ=0.3)	Diff (④-③)/③(%)
y_{sc} (mm)	-212.9627	-213.9041	0.442	-213.6453	-227.0532	6.276
k_{xx}	0.5971	0.5966	-0.089	0.6079	0.6065	-0.230
k_{yy}	0.0463	0.0463	0	0.0526	0.0523	-0.570

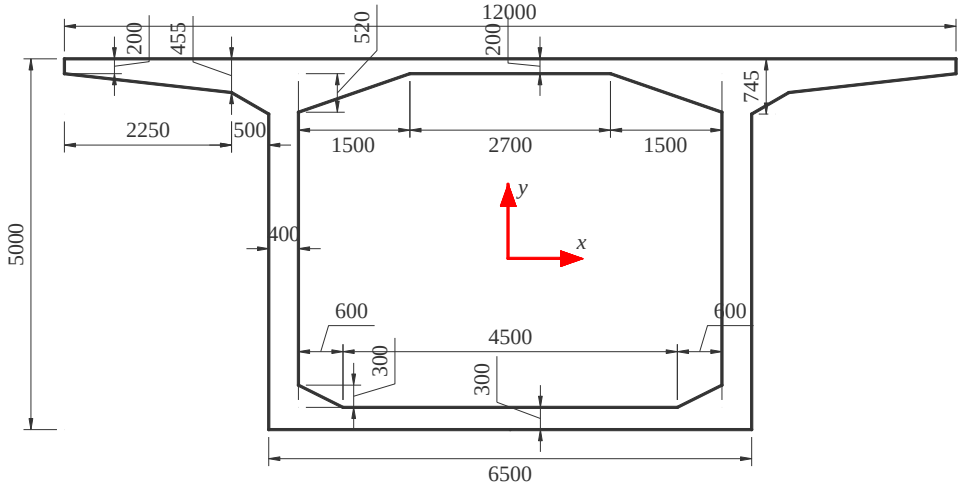

Fig. 14 Dimension of bridge box section

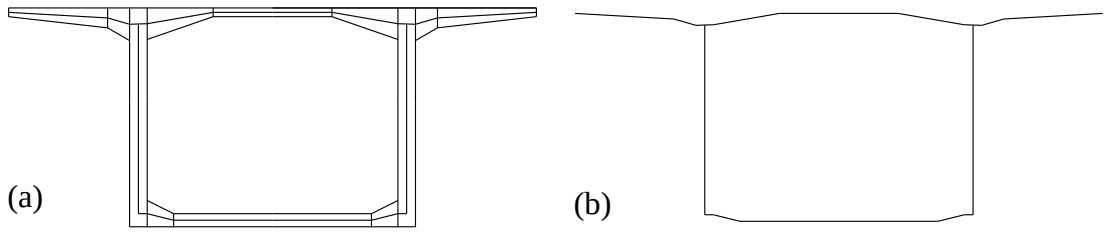

Fig. 15 Modelling of bridge box section: (a) Distribution of taper thicknesses; and (b) 1D warping elements

Table 14
Shear center and shear correction factors of bridge box section

Parameter	①ANSYS (μ=0)	②Present (μ=0)	Diff (②-①)/①(%)	③Warping area element (μ=0.2)	④Present (μ=0.2)	Diff (④-③)/③(%)
y_{sc} (mm)	-625.0437	-662.6341	6.014	-648.2929	-622.3806	-3.997
k_{xx}	0.4297	0.4081	-5.046	0.4368	0.4141	-5.191
k_{yy}	0.3545	0.3209	-9.470	0.3602	0.3250	-9.773

5.5. Example 5 – Large box section with non-uniform thickness

This example is to validate the performance of the proposed method in the calculation of the shear correction factors of the sections with non-uniform thickness. A box section with taper portions at the corners is investigated using the proposed one-dimensional warping element method. As seen in Fig. 15, this kind of box sections are widely used in rail and highway bridges. For economic design with less material as well as reduction of self-weight, the section with taper segments is most welcome. Poisson's ratio is assumed as 0.2 in this example. The modelling for the non-uniform thickness distribution is shown in Fig. 15(a) while the 1D element model by the proposed method is shown in Fig. 15(b). The shear center and shear correction factors from present study are shown in Table 14 against the results from traditional warping area element method allowing for Poisson effect.

From Table 14, it can be observed that the difference for y_{sc} and k_{xx} are less than 5% while k_{yy} is around 10%. The difference may come from the ignorance of the nonuniform shear stress along the plate thickness and the overlapped areas in the intersection points. This example demonstrates the simplicity in modelling and computational efficiency of the proposed method for practical engineering application.

5.6. Example 6 – Built-up double-channel sections

This example shows the application of the presented one-dimensional warping element method in calculating the shear correction factors of thin-walled built-up sections. A double-channel section with configuration listed in Table 15 is investigated. The influence of the distance l_f between two channels and the spacing l_{sp} of fasteners along the longitudinal axis is studied.

Table 15
Parametric study of double-channel section

Section profile	Parameter	Range
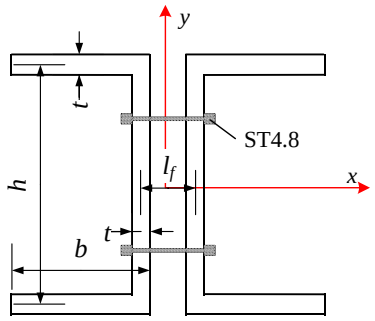	b (mm)	50
	h (mm)	75
	t (mm)	1
	l_f (mm)	2, 5, 10
	l_{sp} (mm)	100, 150, 200
	L/l_{sp}	2 to 11

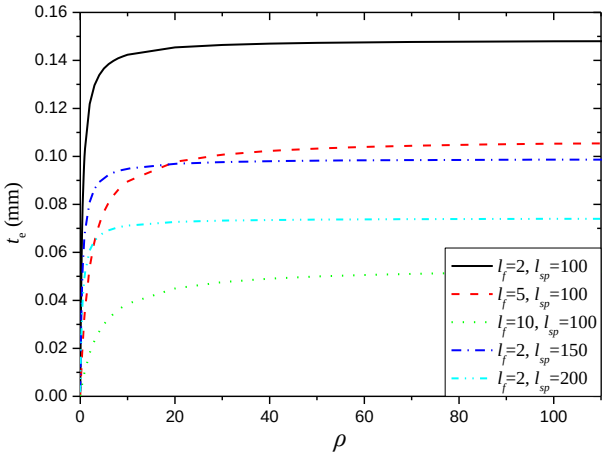

Fig. 16 Influence of rigidity coefficient ρ on the equivalent thickness t_e

The influence on the equivalent plate thickness t_e as given in Eq. (51) due to fixing condition (i.e. rigidity coefficient ρ), distance l_f and spacing l_{sp} is shown in Fig. 16. It can be seen that the equivalent plate t_e decreases with increase of l_f and l_{sp}. It is also noted when the sufficient constraint ($\rho \geq 20$) is provided, t_e approaches $t_{e,max}$ in Eq. (52). In other words, the equivalent plate thickness t_e is significantly affected by the rigidity coefficient ρ ranging from 0 to 20.

As there are few research carried out on the determination of the shear correction factors of built-up sections, no direct results are available for validation of the proposed method. Thus, a finite solid element model for a cantilever beam is employed here for comparison.

Assuming that the shear correction factor k for a general cross section is known, the deflection at the free end of a cantilever beam can be calculated by (Timoshenko 1949):

$$\delta=\delta_b+\delta_s=\frac{PL^3}{3EI}+\frac{PL}{GAk} \tag{61}$$

where, δ_b is due to the bending action; δ_s is due to shear effect.

As shown in Fig. 17(a), a cantilever beam using the built-up double-channel section is studied using the 4-node element SOLID45 in ANSYS. No contact behavior between the surfaces of the adjacent webs of the channels is considered. Only linear elastic analysis is performed. The tip deflection from ANSYS is denoted as δ_{FEM}.

To study the contribution of shear deformation on the total deflection, an indicator β is introduced as below:

$$\beta=\frac{\delta_{FEM}-\delta_b}{\delta_b}=\left(\delta_{FEM}-\frac{PL^3}{3EI}\right)\Big/\frac{PL^3}{3EI} \tag{62}$$

Specifically, δ_{FEM} is the deflection δ_x and δ_y along the x-axis and y-axis respectively as shown in Fig. 17 (b) and (c). The results of β against L/l_{sp} ratio in related to δ_x and δ_y are shown in Fig. 18 and Fig. 19 respectively accounting for different distances l_f and spacings l_{sp}. It is clear that the shear deformation will significantly affect the total deflection of the cantilever beam for $L/l_{sp}<5$ and therefore the shear correction factors should be carefully determined for further global structural analysis, especially in the direct analysis in which the structural responses should be well captured so that the effective length method for stability design is not needed.

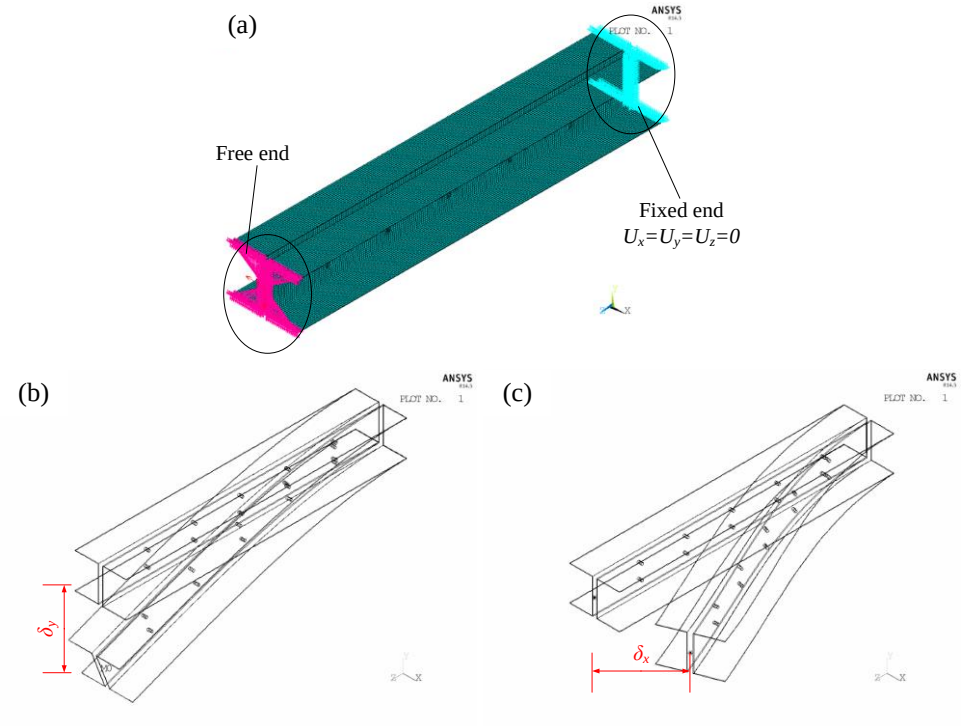

Fig. 17 Finite solid element model for cantilever beam with double-channel section: (a) boundary conditions; (b) vertical deformed shape; and (c) horizontal deformed shape

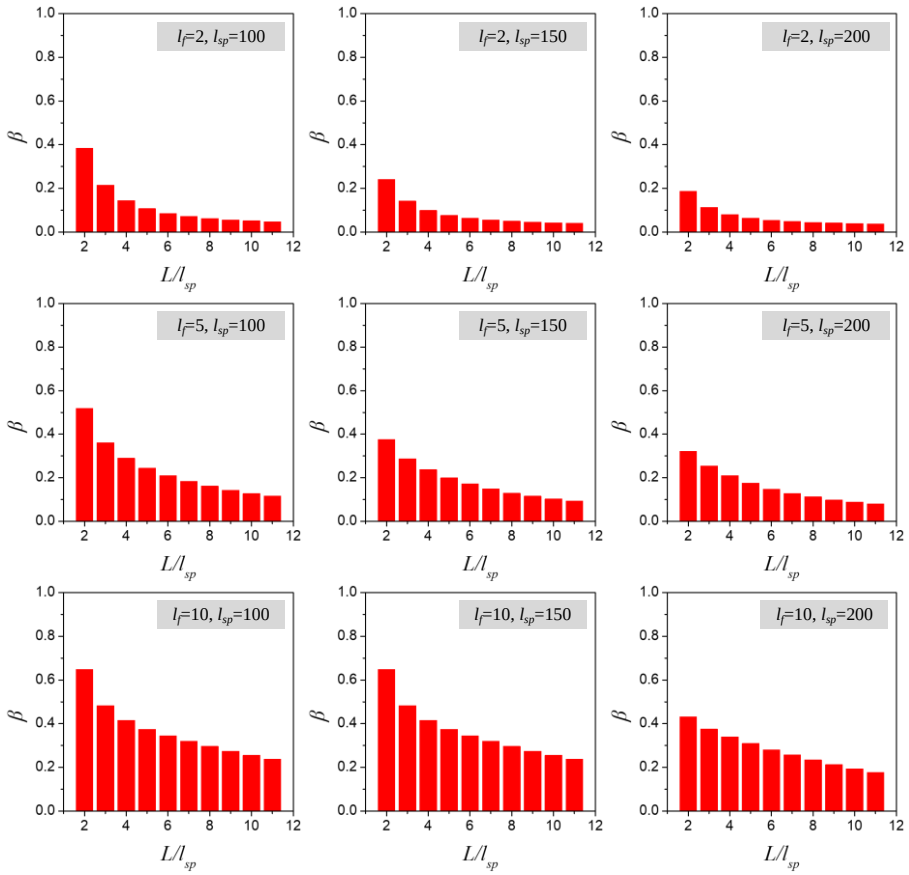

Fig. 18 Change of β in related to δ_x for the cantilever beam

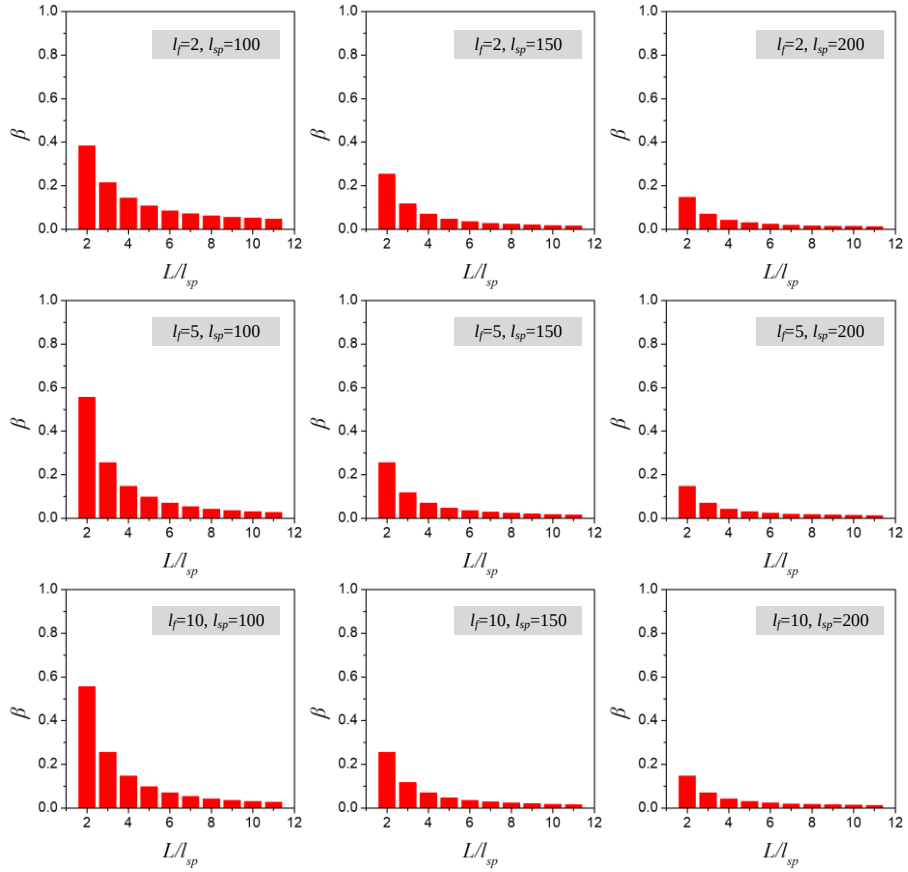

Fig. 19 Change of β in related to δ_y for the cantilever beam

The shear correction factors k_{xx} and k_{yy} of the double-channel sections are calculated by the proposed method and listed in Table 16 and Table 17 respectively. Several fixing conditions (i.e. rigidity coefficient ρ) as well as different distances l_f and spacings l_{sp} have been studied.

From Table 17, it can be found that the shear correction factor k_{yy} along the y-axis of double-channel section is close to the single channel section. The deflections δ_y obtained from the solid finite element model and the analytical solution are listed in Table 18. It can be also seen that there is only slight contribution of composite action along y-direction. Thus, the shear correction factor k_{yy} along the y-axis of the built-up section is almost equal to that of single channel section.

For the shear correction factor along the x-axis, it can be found from Table 16 that the rigidity coefficient ρ shows significant influence on k_{xx}.

Table 16
Shear correction factor k_{xx} of the double-channel sections

ρ	l_f=2			l_f=5			l_f=10		
	l_{sp}=100	l_{sp}=150	l_{sp}=200	l_{sp}=100	l_{sp}=150	l_{sp}=200	l_{sp}=100	l_{sp}=150	l_{sp}=200
($t_{e,max}$)	0.2549	0.2471	0.2397	0.1992	0.1712	0.1501	0.1070	0.0799	0.0637
($t_{e,min}$)	0.1043	0.0595	0.0372	0.0069	0.0031	0.0018	0.0018	0.0008	0.0005
0.01	0.1441	0.1166	0.0979	0.0027	0.0018	0.0013	0.0003	0.0002	0.0002
0.1	0.2368	0.2223	0.2094	0.2368	0.0163	0.0124	0.0033	0.0022	0.0017
1	0.2529	0.2443	0.2363	0.1147	0.0878	0.0711	0.1147	0.0179	0.0136
10	0.2547	0.2468	0.2393	0.1856	0.1564	0.1351	0.0817	0.0593	0.0465
100	0.2548	0.2470	0.2397	0.1978	0.1696	0.1484	0.0817	0.0772	0.0614
Single channel section: k_{xx}=0.4191									

Table 17
Shear correction factor k_{yy} of the double-channel sections

ρ	l_f=2			l_f=5			l_f=10		
	l_{sp}=100	l_{sp}=150	l_{sp}=200	l_{sp}=100	l_{sp}=150	l_{sp}=200	l_{sp}=100	l_{sp}=150	l_{sp}=200
($t_{e,max}$)	0.3276	0.3277	0.3277	0.3260	0.3263	0.3265	0.3249	0.3253	0.3255
($t_{e,min}$)	0.3279	0.3279	0.3279	0.3270	0.3270	0.3270	0.3260	0.3260	0.3260
0.01	0.3279	0.3279	0.3279	0.3270	0.3270	0.3270	0.3260	0.3260	0.3260
0.1	0.3277	0.3278	0.3278	0.3277	0.3270	0.3270	0.3260	0.3260	0.3260
1	0.3276	0.3277	0.3278	0.3267	0.3268	0.3269	0.3267	0.3259	0.3259
10	0.3276	0.3277	0.3277	0.3262	0.3265	0.3266	0.3253	0.3255	0.3256

100	0.3276	0.3277	0.3277	0.3260	0.3264	0.3265	0.3253	0.3253	0.3255

Single channel section: k_{yy}=0.3343

Keeping the spacing l_{sp} as constant (l_{sp}=100), the deflections δ_x obtained from the solid finite element model and the analytical solution are plotted in Fig. 20 to Fig. 22 for l_f = 2, 5 and 10 mm respectively. Clearly, the analytical results with assumption of $t_e = t_{e,max}$ and $t_e = t_{e,min}$ are almost same as the finite element result when l_f = 2mm. It means that when the two channels are too close flexural behavior of the cantilever beam can be well predicted using $t_{e,max}$ or $t_{e,min}$ to compute the shear correction factor.

With the increase of the distance between the two channels (l_f = 5 and 10 mm), the analytical results assuming $t_e = t_{e,min}$ in related to lowest rigidity always predict large displacement than others while the assumption of $t_e = t_{e,max}$ in related to infinite rigidity provides the smallest displacement. The two assumptions are essentially two extreme cases. In reality, the connected details such as plate thickness, bolt size, distance l_f and spacing l_{sp} make the actual rigidity in between the two extreme cases. In this example, ρ = 0.1 and ρ = 1 provide the excellent results with the finite element model for l_f = 5 mm and l_f = 10 mm respectively. In principle, once the rigidity coefficient ρ is determined, the shear correction factors of the built-up section can be obtained. To exactly determine the shear correction factors of built-up sections, more works will be carried out in our future study. This paper aims to provide a good start in the field in which few research was done in previous works.

Table 18
Comparison of deflection along *y*-axis: δ_y

L/l_f	l_f=2, l_{sp}=100				
	①*	②*	③*	Diff (②-①)/① (%)	Diff (③-①)/① (%)
2	0.0573	0.0588	0.0573	-2.622	-2.605
3	0.1558	0.1573	0.1558	-0.915	-0.896
4	0.3376	0.3385	0.3376	-0.267	-0.246
5	0.6305	0.6303	0.6305	0.039	0.061
6	1.0624	1.0601	1.0624	0.220	0.241
7	1.6611	1.6556	1.6611	0.333	0.355
8	2.4545	2.4444	2.4545	0.411	0.433
9	3.4702	3.4541	3.4702	0.466	0.488
10	4.7363	4.7124	4.7363	0.507	0.529
11	6.2804	6.2468	6.2804	0.538	0.560

*: ① δ_y obtained from FEM; ② δ_y obtained by Eq. (61) with t_e=$t_{e,min}$; ③ δ_y obtained by Eq. (61) with t_e=$t_{e,max}$.

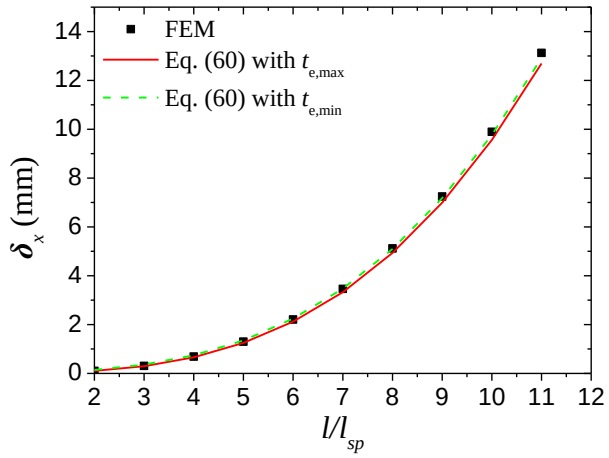

Fig. 20 δ_x of the cantilever with double-channel section: l_f=2 & l_{sp}=100

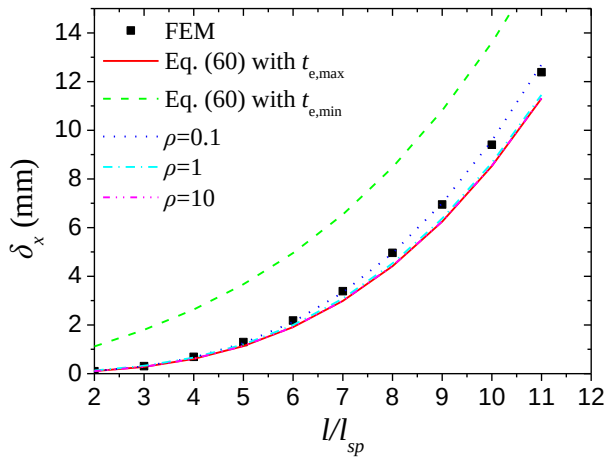

Fig. 21 δ_x of the cantilever with double-channel section: l_f=5 & l_{sp}=100

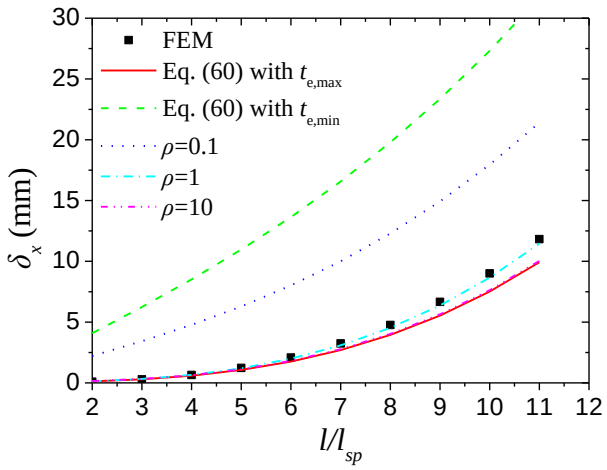

Fig. 22 δ_x of the cantilever with double-channel section: l_f=10 & l_{sp}=100

5.7. Example 7 – Influence of shear deformation in Direct Analysis of steel structures

A single steel member with two different boundary conditions reflecting practical engineering conditions, as shown in Fig. 23 (a) and (b), is studied to demonstrate the influence of shear deformation in the structural analysis of steel structures by using the Direct Analysis Method with consideration of geometric nonlinearity. The steel beam adopts ASTM standard W14x48 section with a length of 8.53 m. The two cases studied are introduced as below:

Case 1: the beam is simply supported with a uniformly distributed load over the length along gravity direction and a concentrated axial force applied at the end of the beam.

Case 2: the beam is fixed at one end and subjected to concentrated forces at the free end.

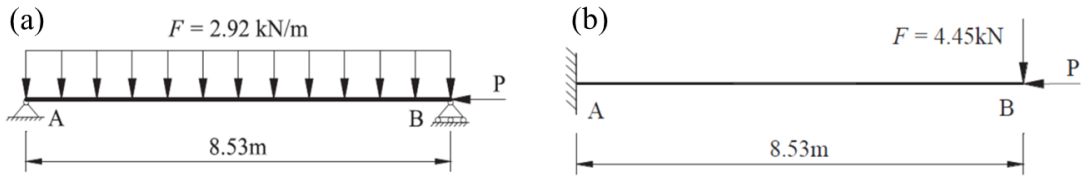

Fig. 23 A single steel member: (a) Case 1 - simply supported; (b) Case 2 - cantilevered

Table 19
Mid-span moment M_{mid} and displacement Δ_{mid} – Case 1

Response	Method	Number of elements	Axial Force, P(kN)			
			0	667	1334	2001
M_{mid} (kN·m)	AISC (2016)	-	26.6	30.5	35.7	43.0
	Du *et al*. (2019)	2	26.56	30.45	35.62	42.89
	SAP2000	2	26.56	30.38	35.46	42.48
		10	26.56	30.45	35.51	42.6
		20	26.56	30.45	35.51	42.6
	Present study (k_{yy} = 0)	1	26.56	26.56	26.56	26.56
	Present study (k_{yy} = 0.3328)	1	26.56	30.44	35.59	42.78
	ANSYS	2	26.558	30.341	35.098	41.259
		10	26.558	30.433	35.583	42.754
		20	26.558	30.437	35.601	42.813
		40	26.558	30.438	35.606	42.828
Δ_{mid} (mm)	AISC (2016)	-	5.13	5.86	6.84	8.21
	Du *et al*. (2019)	2	5.11	5.83	6.80	8.16
	SAP2000	2	5.11	5.82	6.76	8.06
		10	5.11	5.84	6.79	8.11
		20	5.11	5.84	6.79	8.11
	Present study (k_{yy} = 0)	1	5	5.68	6.59	7.85
	Present study (k_{yy} = 0.3328)	1	5.11	5.83	6.79	8.12
	ANSYS	2	5.1065	5.6869	6.416	7.3621
		10	5.1065	5.8256	6.7803	8.109
		20	5.1065	5.8306	6.794	8.1385
		40	5.1065	5.8319	6.7974	8.146

In both cases, the beam is simulated by one advanced beam-column element proposed by Tang *et al*. (2022) with consideration of both initial imperfection and shear deformation. To use this advanced element, the shear correction factor is required and will be calculated by the proposed one-dimensional element method in this paper.

The results are compared with those from AISC (2016), software SAP2000 and ANSYS, and the flexibility-based element from Du *et al*. (2019). The results without consideration of shear deformation (i.e. k_{yy} = 0) are also reported here for demonstration of the influence of shear effect.

Table 19 shows the mid-span moment and mid-span displacement of Case 1. The results are also plotted in Fig. 24 and Fig. 25 for comparison.

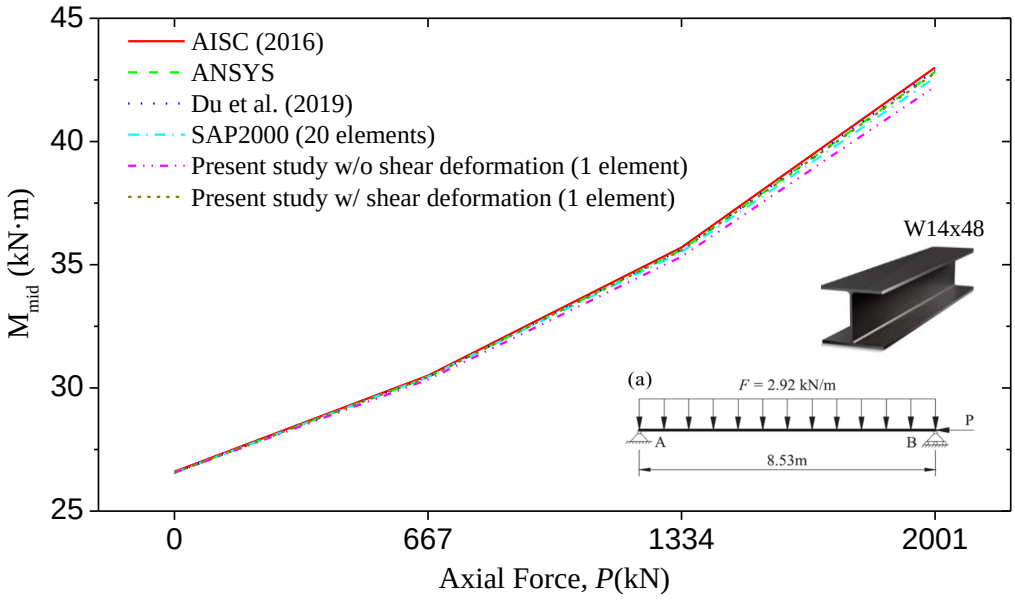

Fig. 24 Moment at mid-span: M_{mid} (kN·m) – Case 1

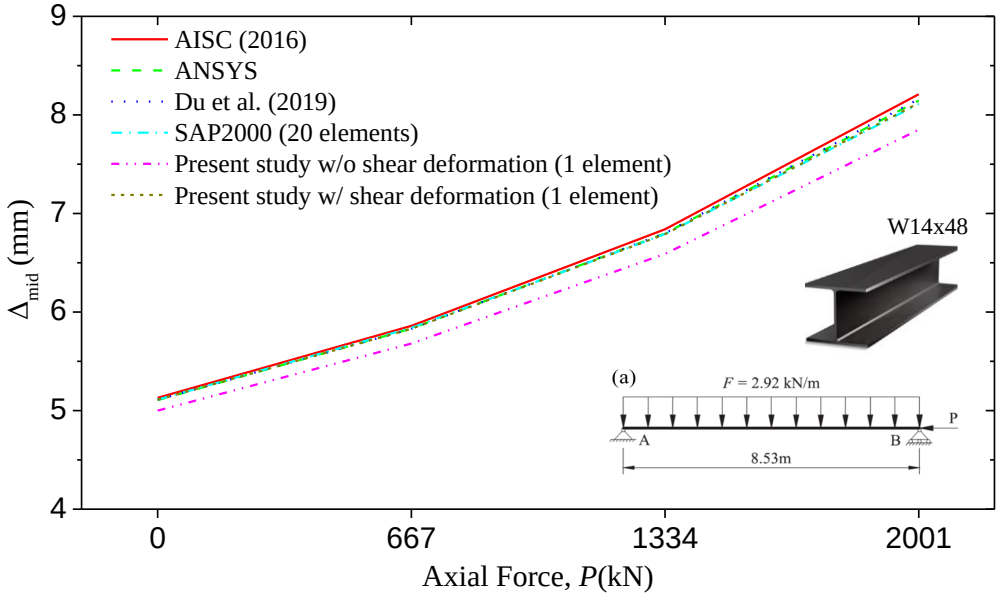

Fig. 25 Displacement at mid span: Δ_{mid} (mm) – Case 1

Table 20
Fixed end moment M_{end} and free end displacement Δ_{end} – Case 2

Response	Method	Number of elements	Axial Force, P(kN)			
			0	667	1334	2001
M_{end} (kN·m)	AISC (2016)	-	38.0	53.2	68.1	97.2
	Du *et al*. (2019)	2	37.96	53.12	67.98	97.37
	SAP2000	2	37.96	53.06	67.71	96.19
		10	37.96	53.10	67.89	96.66
		20	37.96	53.10	67.89	96.66
	Present study (k_{yy} = 0)	1	37.96	52.95	67.49	95.63
	Present study (k_{yy} = 0.3328)	1	37.96	53.10	67.85	96.64
	ANSYS	2	36.06	51.422	66.581	96.695
		10	37.009	52.414	67.619	97.841
		20	37.484	52.9	68.117	98.365
		40	23.1	34.2	45.1	66.6
Δ_{end} (mm)	AISC (2016)	-	23.01	34.08	45.03	66.78
	Du *et al*. (2019)	2	23.01	33.99	44.65	65.39
	SAP2000	2	23.01	34.04	44.86	65.96
		10	23.01	34.04	44.86	65.96
		20	22.85	33.72	44.30	64.83
	Present study (k_{yy} = 0)	1	23.01	34.04	44.84	65.96
	Present study (k_{yy} = 0.3328)	1	23.287	34.664	45.936	68.379
	ANSYS	2	23.287	34.67	45.954	68.431
		10	23.287	34.672	45.958	68.444
		20	38.0	53.2	68.1	97.2
		40	37.96	53.12	67.98	97.37

Table 20 shows the fixed end moment and free end displacement of Case 2. The results are also plotted in Fig. 26 and Fig. 27 for comparison.

It can be observed from both cases that with the axial force increasing, the second-order effect becomes unneglectable and increases exponentially for both moments and displacements. As shown in Fig. 24 to Fig. 27, the difference brought by whether the shear deformation is considered or not becomes more conspicuous and mainly influences the displacement of the structure. It is also noted that the model without consideration of shear deformation will be different from others. The shear deformation adversely impacts structural safety and is thus critical in the Direct Analysis of the structures. In addition, compared with the results from SAP2000 and ANSYS, the proposed one-dimensional method combined with the advanced element proposed by the authors achieves high accuracy while using only one element per member, bringing both modeling and computational efficiency.

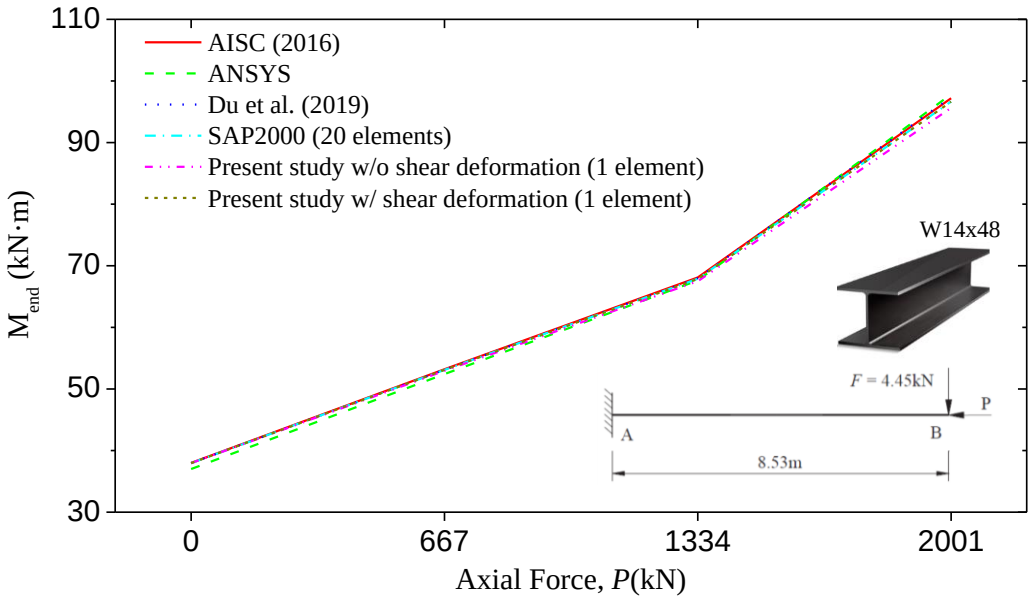

Fig. 26 Moment at fixed end: M_{end} (kN·m) – Case 2

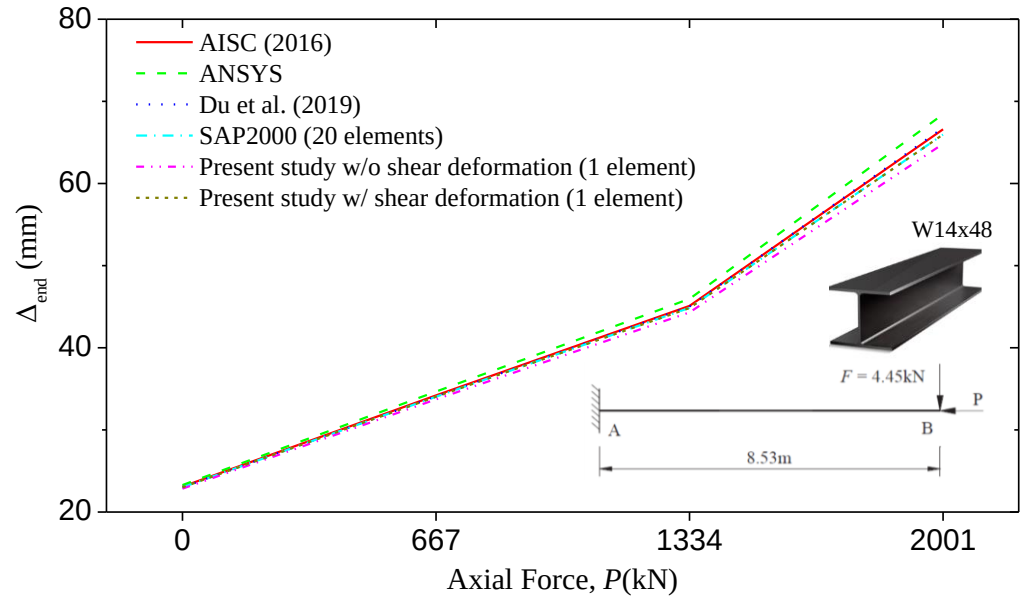

Fig. 27 Displacement at free end: Δ_{end} (mm) – Case 2

6. Conclusions

The shear correction factors of cross sections are required for consideration of shear deformation in global structural analysis such as Direct Analysis Method (DAM) based on beam-column theory. However, there is lack of a general method to determine the shear correction factors of thin-walled cross-sections in various shapes and as a result DAM cannot be applied to the structures adopting these cross-sections. To fill this gap, an innovative one-dimensional warping element model method is proposed to determine the shear correction factors of arbitrary thin-walled sections. The verification examples demonstrate the accuracy and efficiency of the proposed method against the analytical solution, conventional warping area element method and section analysis in ANSYS. The following conclusions can be made from this study:

(1) A one-dimensional warping element model method is proposed to determine the shear correction factors as well as the shear center of the thin-walled cross sections. Only one warping degree of freedom for each end of the proposed element.

(2) The non-uniform plate thickness between the two ends of the element has been taken into account in the element formulation. Thus, the element can be used to find the shear correction factors of the taper sections or the sections with taper portions.

(3) The proposed method can be applied to arbitrary thin-walled sections such as single open and closed sections. The modelling efforts can be significantly reduced for the sections with heavy stiffeners while the computational efficiency can be greatly enhanced.

(4) An equivalent plate thickness method is proposed for the determination of the shear correction factors of built-up sections composed of several single sections. The fixing conditions, distance between individual sections and the spacing of fasteners have been studied.

For the built-up sections, the upper bound and the lower bound of shear correction factors can be obtained by the proposed method. However, as the connected details such as plate thickness, bolt size, distance l_f and spacing l_{sp} will affect the actual rigidity, more research works will be carried out in our future study. Although the influence due to shear deformation on the I-shape section has been preliminarily investigated, more thin-walled members with complicated section shapes will be studied by using the Direct Analysis Method as a future work.

Acknowledgments

The authors are grateful for financial support from the Research Grant Council of the Hong Kong SAR Government on the project "Joint-based second order direct analysis for domed structures allowing for finite joint stiffness (PolyU 152039/18E)", Innovation, Technology Fund for the project “A new membrane-flood gate system for extreme weather hazardous mitigations for use in Hong Kong and worldwide (K-ZPD1)”, the Guangdong

Basic and Applied Basic Research Foundation (No. 2022A1515110289), and the China Postdoctoral Science Foundation (No. 2021M691071).

References

[1] Bai L H, Shen R L, Yan Q S, et al. Progressive-models method for evaluating interactive stability of steel box girders for bridges – Extension of progressive collapse method in ship structures[J]. Structures, 2021, 33:3848-3861.
[2] Shen R L, Bai L H, Zhang S H. Ultimate capacity of narrow type steel box section for railway self-anchored suspension bridge under bias compression. Advanced Steel Construction[J], 2019, 15(2):173–84.
[3] Ljubinkovic F, Martins J P, Gervasio H, et al. Experimental behavior of curved bottom flanges in steel box-girder bridge decks[J]. Journal of Constructional Steel Research, 2019, 160(9):169–188.
[4] Liu S W, Ziemian R D, Liang C, et al. Bifurcation and large-deflection analyses of Thin-walled beam-columns with non-symmetric open-sections. Thin-Walled Structures, 2018, 132:287-301.
[5] Saritas A, Filippou F C. Numerical integration of a class of 3d plastic-damage concrete models and condensation of 3d stress–strain relations for use in beam finite elements[J]. Engineering Structures, 2009, 31(10):2327-2336.
[6] Dikaros I C, Sapountzakis E J, Argyridi A K. Generalized warping effect in the dynamic analysis of beams of arbitrary cross section[J]. Journal of Sound & Vibration, 2016:119-146.
[7] Ding R, Nie X, Tao M X. Fiber beam-column element considering flange contribution for steel links under cyclic loads[J]. Journal of Structural Engineering, 2018, 144(9).
[8] Franza A, Acikgoz S, Dejong M J. Timoshenko beam models for the coupled analysis of building response to tunnelling[J]. Tunnelling and Underground Space Technology, 2020, 96(2):103160.
[9] Wang Y H, Nie J G, Fan J S. Fiber beam-column element for circular concrete filled steel tube under axial–flexure–torsion combined load[J]. Journal of Constructional Steel Research, 2014, 95(4):10-21.
[10] Tao M X, Nie J G. Fiber Beam-column model considering slab spatial composite effect for nonlinear analysis of composite frame systems[J]. Journal of Structural Engineering, 2014, 140(1):04013039.
[11] MSC. Marc Version 2007r1 [Computer software]. MSC, Software Corporation, Santa Ana, CA.
[12] Zhuge H, Xie X. Hysteresis model for fiber elements in effective damaged zone of square-section steel piers considering local instability effect of steel plates[J]. Journal of Structural Engineering, 2020, 146(8):04020156.
[13] Bai R, Hajjar J F, Liu S W, et al. A mixed-field Timoshenko beam-column element for direct analysis of tapered I-sections members[J]. Journal of Constructional Steel Research, 2020, 172:106157.
[14] Du Z L, Ding Z X, Liu Y P, et al. Advanced flexibility-based beam-column element allowing for shear deformation and initial imperfection for direct analysis[J]. Engineering Structures, 2019, 199(15):109586.
[15] Tang Y Q, Ding Y Y, Liu Y P, et al. Innovative displacement-based beam-column element with shear deformation and imperfection[J]. Steel and Composite Structures, 2022, (accepted).
[16] Chan S L, Liu Y P, Zhou Z H. Limitation of effective length method and codified second-order analysis and design[J]. Steel and Composite Structures, 2005. 5(2-3):181-192.
[17] Chan, S L, Zhou Z H. Pointwise equilibrating polynomial element for nonlinear analysis of frames[J]. Journal of Structural Engineering, 1994, 120(6), 1703-1717.
[18] Paolo D R, Daniela A, Filip C. Filippou. Mixed 3D Beam Element with Damage Plasticity for the Analysis of RC Members under Warping Torsion[J]. Journal of Structural Engineering, 2018, 144(6), 04018064.
[19] Daniela A, Paolo D R, Gabriele C. Enriched beam finite element models with torsion and shear warping for the analysis of thin-walled structures[J]. Thin-Walled Structures, 2021, 159:107259.
[20] Timoshenko S P. On the correction for shear of differential equation for transverse vibrations of bars of prismatic bars[J]. Philosophical Magazine, 1921, 41(5):744-746.
[21] Timoshenko S P, Goodier J N. Theory of elasticity[M]. McGraw-Hill, 1970.
[22] Love A E. A treatise on the mathematical theory of elasticity (4th ed.)[M]. Dover Publishing, New York, 1944.
[23] Herrmann L R. Elastic torsional analysis of irregular shapes[J]. Journal of the Engineering Mechanics Division, 1965, 91:11-19.
[24] Cowper, G.R. The shear coefficient in Timoshenko's beam theory[J]. Journal of Applied Mechanics, 1966, 33(2):335–340.
[25] Stephen N G. Timoshenko's Shear coefficient from a beam subjected to gravity loading[J]. Journal of Applied Mechanics, 1980, 47(1):121-127.
[26] Stephen N G. Discussion: "Shear coefficients for Timoshenko beam theory" (Hutchinson, J. R. 2001, ASME J. Appl. Mech. 68, pp. 87-92)[J]. Journal of Applied Mechanics, 2001, 68(6).
[27] Hutchinson J R. Shear coefficients for Timoshenko beam theory[J]. Journal of Applied Mechanics, 2001，68(1):87-92.
[28] Krahula J L, Lauterbach G F. A finite element solution for Saint-Venant torsion[J]. AIAA Journal, 1969, 7(12):2200-2203.
[29] Karan S Surana. Isoparametric elements for cross-sectional properties and stress analysis of beams[J]. International Journal for Numerical Methods in Engineering, 1979.
[30] Schramm U, Kitis L, Kang W, et al. On the shear deformation coefficient in beam theory[J]. Finite Elements in Analysis & Design, 1994, 16(2):141-162.
[31] Friedman Z, Kosmatka J B. Torsion and flexure of a prismatic isotropic beam using the boundary element method[J]. Computers & Structures, 2000, 74(4):479-494.
[32] Gruttmann F, Wagner W. Shear correction factors in Timoshenko's beam theory for arbitrary shaped cross-sections[J]. Computational Mechanics, 2001, 27(3):199-207.
[33] Gruttmann F, Sauer R, Wagner W. Shear stresses in prismatic beams with arbitrary cross-sections[J]. International Journal for Numerical Methods in Engineering, 1999, 45:865-889.
[34] Dong S B, Çarbas S, Taciroglu E. On principal shear axes for correction factors in timoshenko beam theory[J]. International Journal of Solids and Structures, 2013, 50:1681-1688.
[35] Dong S B, Alpdogan C, Taciroglu E. Much ado about shear correction factors in timoshenko beam theory[J]. International Journal of Solids & Structures, 2010, 47(13):1651-1665.
[36] Fialko S Y, Lumelskyy D E. On numerical realization of the problem of torsion and bending of prismatic bars of arbitrary cross section[J]. Journal of Mathematical Sciences, 2013, 192(6):664-681.
[37] Puchegger S, Bauer S, Loidl D, et al. Experimental validation of the shear correction factor[J]. Journal of Sound and Vibration, 2003, 261(1):177-184.
[38] NIDA. User's Manual, Nonlinear Integrated Design and Analysis. NIDA 10 HTML Online Documentation (http://wwwnidacsecom); 2021.
[39] Timoshenko S P, Maccullouoh G H. Elements of strength of materials (3rd ed.)[M]. van Nostrand Co., New York, 1949.